Dynamic Expression of Primary Cilia Across Diverse Human Cancers

Dynamic expression of primary cilia across diverse human cancers

Michael Pei-hong Wu

A thesis submitted in partial fulfillment of
the requirements for the M.D. degree

M.D. Candidate in the Harvard-MIT Division of Health Sciences and Technology

Advisor: Sandro Santagata, MD, PhD
Department of Pathology
Brigham and Women's Hospital
Boston, MA

February 2019

I have reviewed this thesis. It represents work done by the author under my guidance/supervision.

Thesis Advisor

TABLE OF CONTENTS

ABSTRACT

Primary cilia are highly conserved organelles that are best known for their role in signal transduction in development. However, their significance in cancer biology is unclear, with some studies reporting that cilia are lost in cancer while others suggest that cilia promote tumor growth and metastasis. Using immunohistochemistry against the ciliary membrane protein ARL13b, we systematically quantified the cilia found across a diverse spectrum of over 2,000 human tumors. We found that the vast majority of human tumor types were capable of producing cilia, with some tumor types containing more than 50% cells with cilia. Using electron microscopy and live cell imaging, we observed that cilia on tumor cells have atypical ultrastructural features and are highly dynamic, with cilia disassembly immediately before mitosis and re-assembly in the daughter cells. To further investigate the role of cilia in tumor cells, we performed CRISPR/Cas9-mediated knockout of KIF3A in an ovarian cancer cell line. KIF3A knockout resulted in loss of cilia, but without major transcriptomic changes or loss of cell viability. Because cilia have been thought to be features of quiescent or G0/G1 cells, we used multiplexed cyclic immunofluorescence on human tumor samples to characterize the proliferation status of ciliated tumor cells, and found that both proliferating and non-cycling tumor cells were capable of forming cilia.

STATEMENT OF RESEARCH AND ACKNOWLEDGEMENTS

This research project was performed in the laboratory of Dr. Sandro Santagata in the Brigham and Women's Hospital Department of Pathology between the summer of 2016 and December 2018, and represents an ongoing effort to understand the role of cilia in human cancer. This thesis involves the contributions of several members of the Santagata lab. Under the guidance of Dr. Santagata, I designed and performed the experiments and analyzed the data in this thesis unless stated otherwise. Shannon Coy designed experiments and performed the massive undertaking of reviewing the human tumor specimens for the presence of cilia by immunohistochemistry and quantifying the results. Rumana Rashid, Giorgio Gaglia, Ziming Du, and Carmen Li provided invaluable assistance in collecting and analyzing data.

This research would also not be possible without the expertise and support of several collaborating research groups. In the Peter Sorger Lab and the Harvard Laboratory of Systems Pharmacology, Jia-Ren Lin and Peter Sorger, who pioneered the t-CyCIF method, provided crucial guidance with multiplexed immunofluorescence. Clarence Yapp assisted with live cell imaging. Shu-Hsien Sheu, Austin Akey, and Nicki Watson assisted with electron microscopy. Francisca Vazquez performed the computational analysis of gene dependency data from Project Achilles. We also thank Jagesh Shah and his lab members Yinghua Guan and Peter Czarnecki for formative discussions, their expertise in the field of cilia biology, and assistance with live cell imaging and designing CRISPR constructs. We thank Joan Brugge and Ioannis Zervantonakis for their

expertise in ovarian cancer and work with patient-derived xenografts and ovarian cancer cell lines.

The use of human tissues for multiplexed imaging experiments in this study was approved by the Brigham and Women's Hospital Institutional Review Board. This research was supported by grants from the Ludwig Cancer Research Institute and intramural funding from the Brigham and Women's Hospital/Dana Farber Cancer Institute. I was personally supported by a grant from the Harvard Medical School Scholars in Medicine Office, with appreciation to the Herbert R. Morgan, MD-Hans Zinsser, MD Fund for Medical Education. I have no conflicts of interest to declare.

LIST OF ABBREVIATIONS

ARL13b – ADP Ribosylation Factor-Like GTPase 13B

CRISPR – Clustered regularly interspaced short palindromic repeats

EM – Electron microscopy

FFPE – Formalin fixed paraffin embedded

FIB-SEM – Focused ion beam scanning electron microscopy

FUCCI2 – Fluorescent ubiquitination-based cell cycle indicator 2

IFT – Intraflagellar transport protein

IHC – Immunohistochemistry

IMCD – Inner medullary collecting duct (cells)

KIF3A – Kinesin family protein 3A

PCNA – Proliferating cell nuclear antigen

PDX – Patient-derived xenograft

PTCH1 – Patched 1

RPE – Retinal pigment epithelium (cells)

SCLC – Small cell lung cancer

sgRNA – single guide RNA

SHH – Sonic Hedgehog

shRNA – short hairpin RNA

siRNA – small interfering RNA

SMO – Smoothened

SUFU – Suppressor of Fused homolog

t-CyCIF – Tissue-based cyclic immunofluorescence

Wnt – Wingless-related integration site pathway

INTRODUCTION

Overview

Cilia are highly conserved projection-like organelles that extend from the cell surface. Cilia are found widely across all clades of eukaryotic species, suggesting that these organelles are evolutionarily ancient and were present in the last common eukaryotic ancestor[1]. While the structural features of cilia were originally studied in single-celled organisms such as the algae *Chlamydomonas reinhardtii*[2], diverse types of cilia are present in cells throughout the human body and have gained interest in recent years due to increased understanding of their importance in cellular signaling, the cell cycle, and their potential role in human diseases.

In vertebrates, cilia can be divided into motile versus non-motile cilia, which are structurally distinct. In both cases, the cilium consists of a cylindrical projection called the axoneme, which contains a core ring of 9 microtubule doublets. These microtubules emerge out of the basal body of the cilium, which consists of the mother centriole of the cell. However, in motile cilia, there are also 2 central microtubule doublets with associated dynein arms that slide and thereby confer motility to the cilium. This results in a “9+2” arrangement of microtubule doublets in motile cilia, versus the “9+0” arrangement in non-motile cilia. These microtubule structures within the ciliary axoneme are characteristically seen in cross-sectional electron microscopy (EM) images.

In the human body, cilia assume diverse roles. Specialized cell types express multiple motile cilia in order to direct the flow of fluid, with notable examples including the fallopian tube epithelium, the ependymal cells lining the cerebral ventricles, and the respiratory epithelium. A motile single cilium is present on spermatozoa in the form of a flagellum, allowing for directed movement of the spermatozoa. During embryonic development, motile nodal cilia are essential for driving left-right asymmetric development. However, in contrast, solitary non-motile cilia, often referred to as primary cilia[3], are found ubiquitously throughout the human body. While some highly specialized primary cilia serve unique organ-specific functions such as phototransduction in human retinal cells, the role of primary cilia in most human cells is incompletely understood.

Primary cilia and the Sonic Hedgehog and Wnt signal transduction pathways

While primary cilia were formerly considered to be vestigial organelles, in recent years primary cilia have been found to be crucial components of signal transduction pathways. This role of the primary cilium as an “antenna” for signal transduction has been most well established in the context of embryonic development and the Sonic Hedgehog (SHH) signaling pathway. In a mutagenesis screen of mouse embryos for patterning defects, mutations in intraflagellar transport proteins 88 and 172 (IFT88 and IFT172), both of which are known ciliary transport proteins, resulted in abnormal brain morphology with lack of ventral neuronal subtypes, as well as pre-axial polydactyly, phenotypes which

were shown to be due to disrupted SHH signaling[4]. Since this initial discovery of a connection between ciliary proteins and SHH signaling, subsequent biochemical studies have identified the cilium as the locale of SHH signal transduction[5–8]. While SHH signaling is complex and aspects of the pathway remain to be clarified, localization of key effector proteins to the cilium is essential. Briefly, under basal conditions, the Hedgehog receptor Patched (PTCH1) is localized to the ciliary membrane. Upon binding of Hedgehog ligand to Patched, Patched dissociates from the ciliary membrane, and instead, Smoothened (SMO) accumulates in the ciliary membrane. This enables the Suppressor of Fused homolog (SUFU) and Gli proteins to accumulate in the ciliary tip, which frees the Gli proteins from the SUFU:Gli complex and prevents their proteolytic inactivation[8]. The active form Gli proteins then act as transcription factors to induce downstream transcriptional changes associated with the SHH pathway. SHH signaling and its interaction with the primary cilium during development are reviewed in detail by Goetz and Anderson[9].

More controversially, primary cilia have also been implicated in the canonical Wnt signaling pathway. Interestingly, in contrast to the requirement of cilia for SHH pathway activation, knockout of ciliary protein kinesin family protein 3A (KIF3A) results in loss of cilia and increased sensitivity to Wnt signaling[10]. Similarly, knockout of *Dnchc2* in mice was shown to prevent cilia formation and also increased the downstream response to Wnt ligands[11]. Another interesting link between cilia and Wnt signaling has come from the zebrafish development literature. In zebrafish, the protein Inversin has been found to act as a molecular

switch between canonical and non-canonical Wnt signaling pathways[12]. Because Inversin specifically localizes to the proximal portion of the primary cilium, often referred to as a the “Inversin compartment”, this raised the possibility of the cilium acting as a sensor to allow Inversion-mediated switching from canonical to non-canonical Wnt signaling. Ciliated mouse kidney inner medullary collecting duct (IMCD) cells responded to increased fluid flow by increasing Inversin expression, suggesting that primary cilia in these kidney cells may serve as a mechanosensor coupling flow with alterations in Wnt signaling[12,13].

However, the necessity of cilia for canonical Wnt signaling has been called into question by multiple studies. First, it was noted that the developmental phenotypes of mouse mutants with defects in cilia genes do not match those of canonical Wnt pathway mutants[14]. Additionally, expression of Axin2, a well-characterized reporter of Wnt/beta-catenin signaling pathway activation, was normal in mice with mutations in 4 different cilia proteins: IFT172, IFT88, DYNC2H1, and KIF3A. Similarly, zebrafish lacking IFT88 had loss of cilia but had normal canonical and non-canonical Wnt signaling[15]. It has been proposed that the conflicting results of these cilia protein knockout models may be due to cilia-independent functions of classical cilia proteins. In particular, KIF3A has been shown to suppress beta-catenin signaling in non-small cell lung cancer (NSCLC) independent of the presence of cilia[16]. Therefore, while it is clear that notable components of the ciliary machinery are involved in canonical Wnt signaling, the importance of the cilium itself for Wnt signaling remains an area of uncertainty.

Primary cilia and the cell cycle

One of the most interesting aspects of cilia is their relationship to the cell cycle. Early electron microscopy studies noted decreased numbers of cilia in mitotically active rat pituitary gland tissue compared to non-mitotic tissue[17]. Subsequently, it was observed that primary cilia are re-absorbed prior to cell division[18]. These early observations, together with increasing understanding of the molecular mechanisms of cilia disassembly and their interplay with cell cycle effectors, have led to a paradigm that, with a few exceptions, primary cilia are a feature of non-cycling cells[19].

Because the basal body of the primary cilium is the mother centriole, dynamic regulation of ciliogenesis and cilia disassembly is proposed to be coupled to the cell cycle via the centrosome cycle. In order for centrioles to become the basal body, the centrioles must dock at the cell membrane, recruit specialized appendages, and elongate prior to enucleating the ciliary axoneme. Ciliogenesis has been studied in detail using cell culture, where serum starvation and high cell-density conditions reliably induce the production of primary cilia in commonly used cell lines such as NIH 3T3 fibroblasts and retinal pigment epithelium (RPE) cells[18,20]. In proliferative cells, centrosomal proteins Cep97 and CP110 localize to the centrioles and prevent formation of cilia, whereas in quiescent cells, CP110 expression is decreased, permitting formation of cilia[20]. Conversely, when quiescent ciliated cells re-enter the cell cycle, the cilium is disassembled, a process that has primarily been studied by synchronizing cultured cells into quiescence via serum starvation. When serum is re-added to serum-starved

ciliated cells in culture, cilia disassembly classically was described to occur in two waves[21]. The first wave, accounting for cilia disassembly in the majority of cells, occurs during G1, whereas the second smaller wave occurs prior to mitosis. In both instances, it was shown that Aurora A kinase is activated and localizes to the basal body[21]. The activated Aurora A kinase phosphorylates histone deacetylase 6 (HDAC6), which becomes activated to deacetylate tubulin and cause disassembly of the ciliary axoneme. Since Aurora A kinase is also an important regulator of mitotic entry, its additional role at the basal body as a mediator of cilia disassembly offers an attractive mechanism to link cilia with the cell cycle.

The association of cilia disassembly with cell cycle progression has raised the controversial question of whether cilia themselves present a barrier to the cell cycle. Theoretically, the cilium must be dismantled before the centrioles can be repurposed to form the spindle poles necessary for mitosis. However, proving a causal relationship between cilia and the cell cycle has been challenging. Multiple studies have identified proteins that simultaneously promote cilia disassembly/shortening while enabling cell cycle progression. The cilia protein Nde1, for instance, negatively regulates cilia length and knockdown of Nde1 results in not only longer cilia, but also delayed cell cycle re-entry[22]. Similarly, in the developing mouse neocortex, the cilia protein Tctex-1 was shown to promote proliferation and also directly cause cilia disassembly[23]. Perhaps the most convincing evidence for a causal relationship between cilia disassembly and cell cycle progression comes from studies of trichoplein, a keratin intermediate

scaffold protein that localizes to the centrioles, but is reduced at the basal body in serum-starved cells with cilia[24]. Trichoplein was shown to enable Aurora A kinase activation and thereby promote cilia disassembly and cause cell cycle progression beyond G1/S. Notably, when using cells without cilia due to IFT-20 knockdown, additional knockdown of trichoplein failed to prevent cell cycle progression[24]. This suggested that trichoplein's effect of promoting cell cycle progression was dependent on having a cilium to disassemble. Therefore, although a causal relationship remains controversial, some have argued that the disassembly of the primary cilium may serve as a signal to progress through the cell cycle[25,26].

Interestingly, the paradigm of cilia disassembly occurring primarily prior to S phase in order to allow duplication of centrioles has been challenged by advances in live cell imaging models. The development of fluorescent ubiquitination-based cell cycle indicator (FUCCI2) cell lines has enabled live-cell monitoring of cell cycle phase based on differential expression of Cdt1 and Geminin, which are stably expressed in the G1-S and S-G2-M phases, respectively[27]. In contrast to prior studies described above, which traditionally relied on synchronization of cells using serum starvation followed by serum re-addition, analysis of unsynchronized NIH 3T3 cultured fibroblasts showed primary cilia formation not only in cycling cells, but with cilia commonly present as late as G2[28]. This demonstrated that the dynamics of cilia formation and disassembly are more heterogeneous and complex than previously appreciated from serum starvation experiments. As the evidence to-date for cilia dynamics

has predominately come from work in cell culture, it is also evident that the precise relationship between cilia and the cell cycle *in vivo* in human tissue remains to be elucidated.

Primary cilia in human disease and cancer

Genetic defects in cilia proteins lead to several well-recognized human diseases, termed “ciliopathies.” For example, defects in ciliary motility lead to primary ciliary dyskinesia, and defects in cilia genes lead to Joubert, Meckel’s, Bardet-Biedel, and orofacial digital syndromes, among others[29]. Furthermore, several of the defective genes implicated in autosomal dominant and autosomal recessive polycystic kidney disease localize to the primary cilium[30]. Given the ties between primary cilia and the cell cycle and important signaling pathways such as Hedgehog signaling, there is also growing interest in the role of cilia in cancer. Initially, several cancer cell lines were reported to be non-ciliated[31], and it was commonly thought that cilia were lost in tumors due to their high mitotic activity. Compared to normal breast tissue, where cilia are found in both stromal and epithelial cells, malignant and premalignant breast lesions were shown in multiple reports to have marked reductions in cilia expression in both the stromal and epithelial compartments[32–34]. Similarly, while normal pancreatic ductal and acinar cells express primary cilia, cilia were observed to be lost in pancreatic ductal carcinoma[35]. This loss of cilia was recapitulated in a pancreatic cancer oncogenic KRAS mouse model, where the loss of cilia was rescued by treatment with PI3K and MEK1/2 inhibitors, suggesting that unchecked KRAS pathway activity may

be the cause of cilia loss in pancreatic cancer. Additional reports have suggested that primary cilia may also be reduced in a few other solid tumors, such prostate cancer[36], melanoma[37], and epithelial ovarian cancer[38].

In contrast to these reports of cilia loss in solid tumors, a few notable tumors appear to rely directly on expression of primary cilia. Basal cell carcinomas and a subset of medulloblastomas are driven by SHH signaling[39,40]. Constitutive activation of SMO in mouse glial cells activates SHH signal transduction and leads to formation of medulloblastoma tumors, but requires the presence of cilia, particularly the cilia membrane GTPase ARL13b[41,42]. Interestingly, constitutive activation of Gli2, which is downstream of SMO in the SHH pathway, also results in formation of medulloblastoma in mice, but in this case, primary cilia inhibit tumorigenesis. This suggests that primary cilia are instrumental in modulating SHH activity and their role in medulloblastoma tumorigenesis depends on the part of the signaling pathway that is driving tumor growth. This dual role of primary cilia has also been corroborated in basal cell carcinoma[43].

Despite these reports of cilia in individual tumor types, a consensus regarding the presence and role of cilia across the spectrum of human tumors is lacking. While the importance of cilia in SHH-driven tumors has been explored in the past, many human cancers have proven to be resistant to SHH pathway inhibition[44], and it is commonly thought that these tumors do not require cilia and have in fact lost cilia due in part to their high mitotic activity. Here we report a broad, comprehensive characterization of cilia across the majority of human cancer types. We find that cilia are heterogeneously expressed in the spectrum of human tumors, and that

they are stably expressed in both patient-derived xenografts and cancer cell lines. Using live cell imaging of ovarian cancer cell lines, we demonstrate that cilia are expressed dynamically in proliferating tumor cells, but that cilia are nonessential in an ovarian cancer cell line model. Finally, in contrast to prior reports suggesting that cilia are lost in many cancers, we utilize multiplexed immunofluorescence to show that in many cancers, cilia are dynamically expressed in actively cycling tumor cells.

MATERIALS AND METHODS

Cilia quantification in tumors

Formalin fixed and paraffin embedded (FFPE) human tissues were used in accordance with the Partners Human Research Committee. To quantify the frequency of ciliation, immunohistochemistry (IHC) using an antibody against ARL13b (Antibodies Inc., #75-287) was performed on a combination of tumor whole sections and tumor tissue microarrays (TMA). Quantification was performed manually using multiple high-powered fields of view after the entire slide was examined for the presence of tissue regions with ciliated cells.

For quantification of ciliated and proliferating cells by immunofluorescence, tumors were stained using Hoechst, Ki67, PCNA, Arl13b, and gamma-tubulin. Three representative 20x fields of view from each tumor sample were counted manually for cilia (Arl13b positive cilium with a gamma-tubulin positive basal body), and automated counts of total cells and proliferating cells were performed using the Hoechst and Ki67/PCNA stains, respectively.

Cell culture and transfection

For standard growth conditions, Kuramochi human ovarian cancer cells were cultured in RPMI media with 10% FBS and 1% penicillin/streptomycin (complete RPMI) in a 37°C 5% CO2 incubator. For serum modification experiments, the concentration of RBS in RPMI was varied between 0% and 20%. Cells were maintained and passaged every 3-4 days. For transfection, cells were grown in

antibiotic-free medium and then transfected using Lipofectamine 2000 per manufacturer's protocol. Briefly, cells were incubated overnight in transfection medium, after which the transfection medium was aspirated and fresh RPMI with 10% FBS and 1% penicillin/streptomycin was added. 48-72 hours after transfection, the cells were assessed under a fluorescence microscope for GFP expression, then sorted using a FACSAria II Sorter (BD Biosciences), selecting only the top 3% cells by GFP expression. The GFP positive cells were then subcultured either as monoclonal or polyclonal lines. Cells were tested for mycoplasma contamination using the Lonza and ATCC mycoplasma detection kits.

DNA constructs

The L13-Arl13bGFP was a gift from Tamara Caspary (Addgene plasmid # 40879). CRISPR constructs were generated using the pSpCas9(Bb)-2A-GFP backbone vector, a gift from Jagesh Shah. CRISPR constructs were produced using the protocol previously described by Ran and colleagues[45]. Briefly, the single-guide RNA (sgRNA) sequences were designed to target upstream exon sequences of the target genes using the Crispr.mit.edu web tool. sgRNA sequences were ligated into the pSpCas9(Bb)-2A-GFP backbone vector, and the newly made constructs were verified with DNA gels and Sanger sequencing. The pSpCas9(Bb)-2A-GFP vector without any sgRNA sequence was used as transfection control. For full sgRNA construct oligonucleotide sequences, please refer to **Supplementary Table 1**.

Lentivirus packaging and transduction

293T cells were seeded in 10 cm dishes and transfected with the VsVg, delta 8.9, and expression vector of interest using FuGENE6 (Promega) per manufacturer's instructions. At 24 hours post-transfection, the media was aspirated and replaced with fresh DMEM with 10% FBS. Media from 48 and 72 hours post-transfection were collected and filtered through 0.45um filters and stored at -80°C for future use. For lentiviral transduction, the virus-containing media was thawed and added to the target cells with 10 ug/ml polybrene, using multiple different dilutions, optimized to viral titer. The transduction reaction was incubated overnight at 37°C, after which the media was replaced.

Live cell imaging

Cells expressing the L13-Arl13bGFP vector were imaged using a Nikon Eclipse live-cell imaging microscope, the GE IN Cell Analyzer 6000, and the GE DeltaVision Elite microscope. For the Nikon microscope, cells were seeded onto 35 mm MatTek dishes (No. 1.5 glass coverslip). For the IN Cell Analyzer 6000, cells were seeded onto PerkinElmer Cell Carrier 96 well plates. For the Deltavision microscope, cells were seeded onto a chambered coverglass (Thermo Scientific). Temperature and humidity were controlled using a heating chamber. Cells were imaged at varying acquisition intervals (as short as 1 frame every 2 minutes) for 24-48 hours.

Immunofluorescence and cyclic immunofluorescence (t-CycIF)

Using formalin fixed paraffin embedded human tumor samples, microtome sections were made onto glass slides and stored at 4°C until use. Slides were baked, dewaxed, and underwent antigen retrieval using the Leica BOND RX instrument. Immunofluorescence was performed using standard methods. Tissue-based cyclic immunofluorescence (t-CyCIF) is a multiplexed immunofluorescence imaging technique that has been described in detail previously[46,47].

Slides were imaged using either the Zeiss Axio Observer.Z1 inverted fluorescence microscope for standard immunofluorescence imaging, or the Rarecyte and GE In Cell imaging platforms for t-CyCIF. For a complete list of antibodies used in immunofluorescence imaging, please refer to **Supplementary Table 2**.

Electron microscopy

For electron microscopy of the OVSAHO patient derived-xenograft sample, we used an FEI Helios 660 focused-ion beam scanning electron microscope (FIB-SEM) to serially acquire transmission electron microscopy (TEM) images, using the focused ion beam for milling serial sections. Serial sections were used to make 3D reconstructions by first manually tracing subcellular structures using the

VAST software program and then performing the reconstructions using 3D Studio Max software (Autodesk Media and Entertainment).

For conventional TEM of cultured cells, Kuramochi cells were grown to a confluent monolayer in 10 cm and 35 mm dishes, then either fixed in fresh electron microscopy fixative containing glutaraldehyde or scraped gently and pelleted prior to fixation. For imaging cells directed fixed on the tissue culture plate, the walls of the plate were removed prior to imaging. TEM images were obtained by manually cutting and imaging serial sections.

RNA sequencing

RNA from CRISPR knockout and control cells was collected using TRIzol, and purified using the Ambion Purelink RNA Mini kit (Life Technologies). The RNA library construction was performed starting from purified total RNA using the NEBNext Ultra RNA Library Prep Kit for Illumina and the NEBNext Poly(A) mRNA Magnetic Isolation Module (New England Biolabs) according to manufacturer's instructions. The RNA library quality was evaluated using an Agilent Bioanalyzer. Quantification of the libraries was performed using the Kapa Biosystems Library Quantification kit, and libraries were pooled in equal cDNA quantities prior to sequencing on an Illumina NextSeq sequencer. Sequencing data was processed and analyzed for differential expression using the DESeq2 pipeline in RStudio.

siRNA screening

For the list of Silencer siRNA probes (Life Technologies) please refer to **Supplementary Table 3**. siRNA screening was performed using standard methods. Briefly, cells were seeded into 96-well plates at a density of 5,000 cells per well in antibiotic-free medium. Transfection of the siRNAs was performed using Lipofectamine RNAiMax (Life Technologies) per manufacturer's instructions. Fluorescence-tagged non-targeting siRNA was included as transfection controls. For each target gene, 3 different siRNA's were pooled for a final concentration of 30 nM per transfection reaction. The transfection mixture was allowed to incubate 24 hours before changing the media. Quantification of cell proliferation and viability was performed using the CellTiter Glo assay (Promega). Quantification of cilia was performed using immunofluorescence staining for ARL13b and counted manually as described above, and the fraction of ciliated cells was calculated.

In vitro cellular adhesion assay

Cultured cells were trypsinized for 5 minutes, collected in fresh media containing 10% FBS, and pelleted. The cells were counted using a hemocytometer and approximately $1x10^5$ were seeded into each well of 96 well tissue culture-treated plates. At the appropriate timepoints, the media containing unattached cells was removed and the cells were gently washed 4 times with PBS using a multichannel pipette. The remaining cells were fixed in 3.7% formaldehyde and stained with the Hoechst nuclear stain, and imaged on an In Cell Analyzer High

Content Imaging System. Cellular adhesion scores were calculated by dividing the number of adherent cells in 16 fields of view at 20x magnification by the total number of cells seeded into the well.

RESULTS

Tumor cilia and Sonic Hedgehog and Wnt/beta-catenin pathway-driven tumors

Because cilia are known to play important roles in the Sonic Hedgehog (SHH) and Wnt/beta-catenin pathways, we first examined cilia expression in tumors that are predominately driven by these signaling pathways. Medulloblastomas are central nervous system tumors that are divided into 4 molecular subtypes: the Wnt subtype, the SHH subtype, Group 3, and Group 4[40]. While the Wnt and SHH subtypes are driven by mutations resulting in constitutive activation of these pathways, the underlying drivers of malignant proliferation are less clear in Group 3 and Group 4 medulloblastomas. We examined 35 cases of the 4 different subtypes of medulloblastoma tumors using immunohistochemistry against ARL13b, a membrane GTPase that localizes specifically to cilia and is a commonly used marker of cilia. We found that most of the Wnt and SHH pathway-driven medulloblastomas had diffuse expression of cilia (>50% of cells), whereas Group 3 and Group 4 tumors had lower levels of ciliation (**Figure 1A-D**). This correlation between SHH and Wnt pathway activity and cilia expression was also found in other notable tumors. Basal cell carcinomas, which are driven by SHH, as well as adamantinomatous craniopharyngiomas, which are driven by the Wnt pathway, diffusely expressed cilia (**Figure 1E-F**). Therefore, in these tumors with known links to the SHH and Wnt pathways, we found high levels of cilia expression.

We also stained 53 cases of Merkel cell carcinoma and found that a subset of cases had high levels of ciliation, with greater than 50% of cells expressing cilia

(**Figure 1G**). Interestingly, Merkel cell carcinoma is not well known to be associated with SHH or Wnt signaling activity. Therefore, we stained the tumors for beta-catenin, using nuclear localization of beta-catenin as a marker of canonical Wnt pathway activation (**Figure 1H**). Of the 53 Merkel cell carcinoma cases, 6 had nuclear beta-catenin. The presence of beta-catenin localization in the nucleus was associated with higher levels of cilia expression ($p = 0.03$). Therefore, in Merkel cell carcinoma, as in other more-well studied tumors, expression of cilia is correlated with high levels of Wnt/beta-catenin pathway activation.

Characterization of cilia across human cancer types

In addition to examining tumors where SHH and Wnt/beta-catenin signaling have been strongly implicated in pathogenesis, we also sought to broadly characterize the landscape of cilia expression across the major human tumor types. We examined 2,041 human tumor cases across 36 different tumor types using immunohistochemistry against ARL13B to visualize cilia (**Figures 1I, 2A-B**). Cilia were found across a wide range of human tumor types and organ systems. Craniopharyngiomas were the tumor type with the greatest number of ciliated cells, with all cases having greater than 50% cells with cilia. Other highly ciliated tumor types were basal cell carcinoma, granulosa cell tumors, and papillary thyroid cancer. Of the 36 tumor types surveyed, 23 had at least one case with greater than 50% cells ciliated. Several tumor types had a wide variance in the percentage of cells with cilia. For example, among high grade serous ovarian

carcinomas, the percentage of ciliated cells ranged from 0% to greater than 80% across different patient cases. Similar diversity of ciliation, from 0% to greater than 50% ciliation, was found in several other tumor types including glioblastoma, diffuse large B cell lymphoma, small cell lung carcinoma (SCLC), and melanoma.

The least ciliated tumor types were hepatocellular carcinoma, chromophobe renal cell carcinoma, breast carcinoma, all of which uniformly had less than 20% ciliated cells. Pancreatic adenocarcinoma was also notable for its low level of ciliation. However, while previous reports have described that primary cilia are lost in the development of pancreatic adenocarcinoma[35,48,49], we did find one case of pancreatic adenocarcinoma with ciliated tumor cells.

Of note, multiciliated tumor cells were commonly observed in select tumor types: ependymoma, glioblastoma, low and high grade serous ovarian carcinoma, and endometrial adenocarcinoma (**Figure 3**). Furthermore, rare cases containing multiciliated cells were also found among the following tumor types: lung adenocarcinoma, papillary thyroid carcinoma, clear cell renal cell carcinoma, malignant melanoma, and cholangiocarcinoma. Additional distinctive and unusual features of cilia were also noted in a few tumor types. Cholangiocarcinoma tumor cells were organized in nests forming a central lumen, with markedly long cilia pointed inwards toward the lumen. Meanwhile, ARL13B staining in oligodendrogliomas highlighted linear structures spanning the nucleus of the cell (**Figure 3E**). Taken together, these findings illustrate the broad extent of cilia expression in human tumor tissue, as well as the diversity of types of cilia.

Cilia are maintained after treatment and in patient-derived xenografts

Given that the level of ciliation varied considerably across different patient cases of the same tumor type, we asked whether the tendency to form cilia is intrinsic to certain cancer cells or primarily driven by environmental factors. We found that ciliated high grade serous ovarian carcinomas continued to express cilia after treatment with standard chemotherapy (carboplatin with paclitaxel), suggesting that the ciliated cellular phenotype is not eliminated by chemotherapy (**Figure 2C-F**). Furthermore, we examined patient-derived xenograft (PDX) tumors in which patients' ovarian tumor cells were taken directly from the operating room at the time of resection and implanted into mice via either injection into the peritoneal fluid or injection directly into the omentum. The tumor cells injected into the peritoneum formed malignant ascites, whereas the tumor cells injected into the omentum formed solid tumors, thereby creating an invasive disease model (**Figure 2G-J**). We examined 15 PDX models, each containing malignant ascites and invasive omental disease. Similar to native human high grade serous ovarian carcinomas, the tendency of PDX tumor cells to form cilia ranged from less than 10% ciliated cells to greater than 50% ciliated cells (**Figure 2K**). Furthermore, when grown as ascites, the tumor cells had lower ciliation as compared to tumor growing as invasive disease in the omentum in all 15 PDX cases ($p = 0.003$). Of the ascites models, 10 of 15 PDX's had less than 10% cells with cilia. Nevertheless, the relative tendency of each individual PDX to form cilia remained consistent: tumors that were highly ciliated in the invasive form also

tended to have greater ciliation when grown as malignant ascites compared to other PDX malignant ascites cells. For example, the most highly ciliated ascites PDX models were M8, M6, and M4. These three cases were also among the most ciliated PDX's when grown as invasive omental disease, with greater than 40% of cells bearing cilia. This indicates that while environmental factors do affect the rate of ciliation, there is nevertheless a tumor cell-intrinsic tendency to either form or not form cilia.

Ultrastructural features of tumor cilia

In order to characterize the ultrastructural features of these cilia, we performed electron microscopy on human high grade serous ovarian carcinoma cells. We examined patient tumor cells grown as PDX as well as in cultured high grade serous ovarian cancer cell lines. Classically, primary cilia are characterized by an axoneme with a cross-sectional appearance of 9 outer microtubule doublets, with no central microtubules (a 9+0 architecture), whereas motile cilia have two central microtubule singlets (a 9+2 architecture) with dynein arms. In both the PDX tumors and cancer cells lines, we observed the canonical 9+0 microtubule doublet architecture without evidence of dynein arms, consistent with non-motile primary cilia (**Figure 1J-K**). FIB-SEM was used to perform TEM-based 3D reconstructions of cilia arising out of the basal body (**Figure 1M**). However, aberrant axonemal organizations were also frequently observed in the cultured ovarian cancer cell lines. In Kuramochi cells, where TEM with serial sectioning allowed for cross-sectional characterization of 8 tumor cilia, 2 cilia had 6 outer

microtubule clusters and 4 cilia had 7 outer microtubule clusters, as opposed to the classic 9 outer microtubule doublets most commonly described in mammalian primary cilia. In 1 case, the outer microtubule clusters were composed of 4 microtubules each rather than doublets (**Figure 1L**). Furthermore, several cilia contained either central electron dense structures or central microtubules, a feature normally found in motile cilia. 3 out of 8 Kuramochi cilia cross-sections contained 2 central microtubules and 2 out of 8 cilia contained 3 central microtubules. As a result, these multiple aberrancies led to unconventional axonemal organizations of microtubules such as 7+2, 7+3, and 6+2 in addition to the expected 9+0 configuration. Therefore, the solitary tumor cilia described conformed to neither the traditional structural patterns described for primary cilia nor the structure of motile cilia.

Cilia are non-essential in human ovarian cancer cell lines

While the presence of cilia in tumors driven by SHH and Wnt/beta-catenin signaling can be explained by the important roles that primary cilia play in these pathways, we found that cilia were expressed by many other types of human tumors. Many of these malignancies are not known to be primarily dependent on SHH or Wnt signaling, such as high grade serous ovarian carcinoma, glioblastoma, and SCLC. In order to determine if cilia play an important functional role in these tumors, we focused on cell culture models of high grade serous ovarian carcinoma.

We examined five different ovarian cancer cell lines for cilia using immunofluorescence staining for ARL13B as a marker of the ciliary membrane (**Figure 7A**). Of these cell lines, OVSAHO and Kuramochi had the highest percentage of ciliated cells, 32% and 46% cells ciliated when grown under normal culture conditions with 10% fetal bovine serum (FBS), respectively. Interestingly, a comparison of the mutations and copy number alterations in 47 ovarian cancer cell lines found that Kuramochi and OVSAHO were the most similar to high grade serous ovarian tumors[50], suggesting that the high ciliation in these cell lines is less likely to be an artefact of genetic drift in cell culture. 72 hours of serum starvation increased the fraction of ciliated cells in all of the cell lines (**Figure 7B**). Even the cell line OV90, which produced little to no cilia under normal growth conditions with 10% FBS, was able to produce occasional short cilia under serum starvation conditions.

Next we sought to determine the effects of cilia knockdown in these cell lines. We performed siRNA-mediated knockdown against 22 different genes that have been implicated in cilia formation and maintenance. Partial reduction in the fraction of ciliated cells was observed with knockdown of several genes, with up to 78% reduction in the fraction of ciliated cells when knocking down NEK3 or CEP164 (**Figure 4A**). Transient knockdown of CEP164, KIF24, ODF2, AURKA, NEK5, NEK7, NEK8, and NEK9 independently resulted in decreased cell proliferation relative to control, but several of these genes are known to be important regulators of the cell cycle independent of their role in cilia (**Figure 4B**). Furthermore, the degree of cilia reduction did not correlate with reduction in

proliferation, suggesting that the changes in cell growth in knockdown conditions may be accounted for by mechanisms other than cilia loss.

To investigate whether stable complete loss of cilia would affect the growth of tumor cells, we used the CRISPR/Cas9 system directed against Kinesin Family Protein 3A (KIF3A) to generate 4 monoclonal cell lines derived from the Kuramochi parental cell line. As a control, 4 monoclonal lines without the guide RNA targeting KIF3A were also produced in parallel. CRISPR/Cas9-mediated knockout of KIF3A resulted in complete loss of cilia in 3 monoclonal cell lines and partial loss of cilia in 1 monoclonal cell line (**Figure 5A-B**). The KIF3A CRISPR line with partial loss of cilia, referred to as KIF3A 1, expressed sparse short length cilia. Compared to the control-transfected monoclonal cell lines, the KIF3A CRISPR cell lines did not have statistically significant differences in doubling times (**Figure 5E**, $p = 0.4$), and were stably grown in culture for multiple passages.

To evaluate the consequences of loss of cilia on downstream gene expression, we performed RNA sequencing of the KIF3A CRISPR monoclonal cell lines and the control monoclonal cell lines (**Figure 5C-D**). The resulting transcriptomic data was analyzed for changes in major gene ontologies and pathways as defined by the Kyoto Encyclopedia of Genes and Genomes (KEGG) online database. Compared to the control cell lines, 2 KIF3A CRISPR cell lines with complete cilia knockout showed statistically significant changes after correction for false discovery rate in only 1 KEGG gene pathway, “olfactory transduction” (hsa04740). This pathway was upregulated in the KIF3A knockout compared to

control (q = 0.0001). Of note, while the KEGG pathway “ECM-receptor interaction” (hsa04512) had no significant differences (q = 0.99), a subset of genes in this pathway including ITGA3, ITGA4, ITGA5, ITGB3, and LAMC2 were upregulated in the KIF3A knockout lines compared to control. There were no statistically significant downregulated KEGG pathways. Overall, clonal variation between the different monoclonal cell lines accounted for more of the transcriptomic differences than any differences between aggregated control and KIF3A knockout group data, resulting in inconsistent patterns of transcriptomic changes between the two groups.

We also analyzed gene dependency data from the Achilles Project, a large-scale project aimed at characterizing gene dependencies in cancer using a library of hundreds of different cancer cell lines[51,52]. We selected a set of well-validated cilia genes and searched for associations between expression of this gene set and dependency on genes knocked out in the Achilles dataset. We found that cell lines expressing high amounts of cilia genes were dependent on a few cell adhesion-related genes including ITGAV, FERMT2, and PTK2 for viability (**Figure 6**). To determine if cilia knockout resulted in any changes in cellular adhesion phenotype, we performed *in vitro* adhesion assays and found that only one of the KIF3A knockout cell lines had statistically significant increased rates of adhesion compared to the control cell lines (**Figure 5F**). Therefore, while expression of cilia may be linked to changes in genes related to cellular adhesion, the knockout of cilia did not have clear phenotypic significance in these ovarian cancer cells.

Interestingly, there were also no consistent changes in Wnt/beta catenin pathway or SHH pathway gene expression in the KIF3A CRISPR knockout Kuramochi cells compared to control. However, at baseline, the activity of these pathways in the parental Kuramochi cell line is low, suggesting that the presence of cilia in these cell lines is not primarily driven by signal transduction in these pathways as it is in tumors such as medulloblastoma and basal cell carcinoma.

Cilia are dynamically expressed in cycling cells

The formation, maintenance, and reabsorption of primary cilia have been reported to be closely linked to the cell cycle[25]. In order to better characterize the dynamics of cilia in cycling tumor cells, we transduced Kuramochi and OVSAHO ovarian cancer cells with lentivirus containing the ARL13b-eGFP expression construct. Live cell imaging of these ARL13b-eGFP expressing cells revealed that cilia are expressed by cycling cells and are disassembled before mitosis (**Figure 7C-D**). The timing of cilia disassembly was heterogeneous. We tracked 15 cilia disassembly events using live cell imaging and observed that the time from complete cilia disassembly to mitosis ranged from 8 minutes to 264 minutes. 5 of the 15 disassembly events occurred within 1 hour of metaphase. This loss of cilia before mitosis was consistent with immunofluorescence of fixed cells, in which most of the cells in M phase did not have visible cilia. However, we did note occasional cells actively undergoing cytokinesis while still expressing a cilium, both in culture and in human tumor tissue (**Figure 7E-G**), suggesting that

in some cancer cells, dysregulation of the cell division process may result in failure to reabsorb the cilium prior to mitosis.

We also observed bi-ciliated cells in which two cilia appeared to arise from the same base on the cell (**Figure 7H**, **Supplementary Video 1**). These bi-ciliated cells often had multiple nuclei, suggesting a defect in control of DNA replication and cell division. Finally, using live cell imaging of the OVSAHO and Kuramochi Arl13B-EGFP cell lines, we observed events in which the tip of the cilium spontaneously became detached and was released prior to mitosis (**Figure 7I, Supplementary Video 2**). Interestingly, focused ion beam serial transmission electron microscopy (FIB-SEM) of human OVSAHO patient-derived xenograft cells revealed vesicle-like structures associated with the cilium (**Figure 7J**). Recent reports have described this phenomenon of ciliary tip excision and fragmentation and linked it to proliferative effects and drug resistance[26,53,54]. Our data corroborate the presence of this phenomenon and highlight the dynamic nature of cilia expression in cycling cancer cells *in vitro*.

Cilia are expressed by actively cycling tumor cells in human surgical tumor specimens

Given the relationship between cilia and stages of the cell cycle in culture, we sought to better understand the cell state of the ciliated cells within human tumors. We utilized tissue-based cyclic immunofluorescence (t-CyCIF) in order to ask whether cilia are found on tumor cells that are active in the cell cycle in human surgical tumor specimens[47]. For this detailed analysis, we selected once

case each of glioblastoma, a high grade serous ovarian cancer brain metastasis, lung adenocarcinoma, and a SCLC brain metastasis because of the relatively high ciliation in these prevalent and highly mitotic tumors. In order to distinguish tumor cells from stromal elements, we used the following tumor markers: pan-cytokeratin (ovarian cancer, lung adenocarcinoma, and SCLC), PAX8 (ovarian cancer), SOX2 (glioblastoma), and GFAP (glioblastoma). We used antibodies against Ki-67 and proliferating cell nuclear antigen (PCNA) to identify actively cycling cells, and used phospho-histone H3 as a marker of M phase cells. By aligning and segmenting the images of tumor tissue as described by Lin and colleagues[46,47], we were able perform an preliminary analysis of cell cycle activity in over 1,000 single tumor cells in each of the 4 different surgical tumor specimens.

In all of the tumor specimens, the percentage of tumor cells positive for PCNA was greater than the percentage of tumor cells positive for Ki-67. In the glioblastoma case, for example, 24% of all tumor cells expressed Ki-67 while of 39% expressed PCNA (**Figures 8, 9**). Tumor cells expressing Ki-67 also expressed PCNA, but not vice versa, suggesting that Ki-67 is a more stringent marker of cell cycle activity than PCNA. We therefore focused on Ki-67 as a marker of proliferation. The most proliferative tumor case was SCLC, with 34% Ki-67 positive tumor cells, and the least proliferative tumor was the lung adenocarcinoma, with 4% Ki-67 cells. As these tumor cases were selected for their presence of cilia by IHC, they also showed high rates of ciliation by immunofluorescence, with 47% tumor cells expressing cilia in glioblastoma, 74%

in the high grade serous ovarian carcinoma, 44% in the SCLC, and 84% in the lung adenocarcinoma. In all 4 tumor cases, ciliated tumor cells were observed expressing cilia. In the case of SCLC, the percentage of ciliated tumor cells expressing Ki-67 was as high as 48%. Ciliated cells expressing phosphor-histone H3 were extremely rare. This indicates that actively proliferating tumor cells are capable of producing cilia, and that maintenance of the cilia during M phase is rare in human tumor tissue. Therefore, consistent with cell culture models of cilia in cancer cell lines, expression of cilia in human tumor tissue is dynamic and varies with the cell cycle.

DISCUSSION

The role of cilia in human tumors

The presence of cilia in cancer has been reported independently in several different tumors, including medulloblastoma, basal cell carcinoma, craniopharyngioma, glioblastoma, and melanoma, but a broad quantitative analysis of cilia in human cancer has been lacking[41,43,53,55,56]. Using ARL13b as a marker of cilia, we characterized the ciliation status of 36 different human tumor types and 2,041 individual tumor cases, representing the most comprehensive description of cilia in human tumors to date. We found that certain tumors, such as craniopharyngiomas, basal cell carcinomas, and granulosa cell tumors, had a propensity to be highly ciliated, whereas others, such as hepatocellular carcinoma, rarely expressed cilia. However, surprisingly, there was a large variance in the percentage of ciliated cells within individual tumor types, such as in glioblastoma, high grade serous ovarian cancer, and the lung carcinomas. This finding raises the important questions of whether these cilia play an important role in these tumors and whether the highly ciliated tumor cases represent molecularly distinct subclasses of tumors, as we found in medulloblastoma tumors driven by SHH and Wnt/beta-catenin signaling and in Merkel cell tumors with activated Wnt/beta-catenin signaling. However, in most of the tumor types examined, there was no clear way of predicting which tumors would highly express cilia and which would not. Controversially, the oncogenic growth factor receptors EGFR and PDGFR have been reported to localize to the primary cilium[57,58]. A next step in further investigating the role of cilia in tumors would be

to correlate EGFR and PDGFR mutation status with cilia expression in tumors such as lung adenocarcinoma and gastrointestinal stromal tumors.

A potential role for cilia in high grade serous ovarian carcinoma is particularly intriguing because it is a cancer that is not known to be driven by SHH or Wnt signaling and is a prevalent, aggressive disease with high morbidity and mortality. In contrast to previous reports that epithelial ovarian cancers have reduced numbers of primary cilia[38], we found that the expression of cilia in high grade serous ovarian carcinoma is heterogeneous. However, even in the highly ciliated and well-validated Kuramochi ovarian cancer cell line, complete cilia knockout using CRISPR/Cas9 targeting KIF3A did not consistently produce significant transcriptomic changes or changes in growth rate. It is possible that knockout of cilia induced transient transcriptomic or phenotypic changes that we were unable to capture using our experimental design. Because we utilized monoclonal knockout and control cell lines, each cell line was grown for multiple passages in order to generate a population of cells from a single sorted cell. These multiple passages may have allowed for selection of cells with multiple redundancies in growth factor signaling pathways that compensate for reduced input signaling from the absent cilium. It is, however, worth noting that the cilia knockout phenotype was stable over the course of these multiple passages, indicating that even if compensatory signaling pathways were upregulated, they stably did not require the presence of cilia.

Overall, this suggests that in high grade serous ovarian cancer, primary cilia are highly expressed in some cases but nevertheless may be neither a requirement

nor impediment to growth. This contrasts with recent and contradictory findings in other tumors. In gliomas, cilia have been reported to promote growth through excision of cilia tip vesicles[53], whereas in melanoma loss of cilia has been proposed as a driver of tumorigenesis[56]. Furthermore, cilia have been implicated in kinase inhibitor resistance in cell culture models of non-small cell lung cancer and rhabdomyosarcoma[54]. It is possible that the seemingly contradictory roles of cilia in these various tumor types reflect the fact that the cilium is an ancient organelle that can have very different purposes for different tissue types, including varying roles in different types of tumors. Finally, our finding of non-canonical axoneme microtubule arrangements in ovarian cancer cells lines mirrors the literature in glioblastoma, where ultrastructural perturbations in cilia have been reported[59]. Future work directly comparing the axoneme structures in diseased versus health human tissue will be required to clarify whether these atypical structural characteristics are a specific feature of malignancy or if they represent a less well-appreciated normal variant.

Cilia and the cell cycle

While it is recognized that the expression of cilia is coordinated with the cell cycle, the implications of this link have remained an area of debate, particularly in human tissue. Experiments in synchronized human cultured cells have shown that trichoplein and Aurora A kinase cause a large wave of cilia disassembly prior to the G1/S transition[21,24], leading to the paradigm that cilia are largely a feature of the G0 or G1 states. However, advances in single cell live cell imaging have

revealed that in unsynchronized cultured cells, cilia are commonly found throughout G2, with disassembly occurring close to cytokinesis[28]. Our own live cell imaging data in ovarian cancer cell lines are consistent with this finding, as we observed heterogeneous patterns of cilia disassembly, with complete loss of the cilium occurring as late as 8 minutes before metaphase. This further challenges the popular belief that cilia disassembly is a prerequisite for the duplication of the centrioles during S phase. As Ford and colleagues have recently proposed, it is likely that in ciliated S phase cells, the mother centriole maintains its role as the basal body while the centrioles are duplicated[28].

The ability of the cilium to be maintained throughout the S and G2 phases of the cell cycle in cultured cells also suggests that loss of ciliation is not a reliable marker of proliferative activity in human tissue. This is consistent with our findings in high grade serous ovarian cancer, glioblastoma, SCLC, and lung adenocarcinoma, where ciliated cells were consistently found to also be actively proliferating using multiple markers of proliferation. Indeed, the fact that high degrees of ciliation were found in cases of these highly aggressive tumor types further suggests that the presence of cilia are not necessarily a sign of quiescence. Future studies at the single cell level will enable better characterization of the cell state of the ciliated tumor cells and may shed further light on the role these dynamic organelles play *in vivo*.

More broadly, this study demonstrates the importance of quantitative, large-scale analysis of human tissue in the study of cancer biology. Prior studies have reported loss of cilia in multiple cancer types such as melanoma[37] and ovarian[38]

and prostate cancer[36], but in our broad survey of human cancer we found that even in these malignancies notable levels of ciliation were observed. Much of the understanding of cilia to date has come from cell culture models. While cell culture experiments have and will likely continue to provide valuable insights into the molecular composition and signaling pathways of the cilium, it is also clear that cilia are dynamically regulated and are influenced by the surrounding environment and conditions such as serum starvation. In contrast to cell culture, the human tumor microenvironment is highly variable, and differences in cilia expression in human tissue may be attributable to differences in the microenvironment. For example, specifically in ovarian cancer, we found that ascites tumor cells had a lower frequency of cilia compared to tumor cells implanted into solid tissue, suggesting that either lack of cellular adhesion to a solid substrate and subsequent development of polarity or the presence of factors within the ascites milieu inhibit cilia growth. It is possible that other environmental factors affect ciliogenesis within the tumor microenvironment, making it all the more important to study tumor cilia within the context of human tissue. Future work is needed to better understand what factors promote the formation of cilia and whether these factors can account for differences in cilia frequency in surgical tumor specimens.

CONCLUSIONS

In summary, we performed a broad characterization of cilia in human cancers and found diverse patterns of cilia both within and between tumor types, including tumors that had previously been reported to have cilia loss. These tumor cilia resemble classical primary cilia but can exhibit aberrancies in microtubule structure. In medulloblastoma, basal cell carcinoma, and Merkel cell carcinoma, SHH and Wnt/beta-catenin pathway activation is correlated with increased cilia frequency. However, in the majority of tumors, clues regarding the molecular drivers of ciliation remain to be found. We found that complete knockout of cilia in a high grade serous ovarian cancer cell line produced few consistent transcriptomic changes by RNA-sequencing, and that cilia are non-essential in this cell line.

Contrary to the popular belief that cilia are mostly present in the G0/G1 phases of the cell cycle, we found that in ovarian cancer cell lines, cilia are consistently found within 1 hour prior to mitosis. Furthermore, in human tumor tissue, ciliated tumor cells express Ki-67 and PCNA, indicating that ciliated cells are active in the cell cycle. Together with other recent studies, this result indicates that while the expression of cilia is coordinated with the cell cycle, the presence or absence of cilia in tumor tissue does not reflect the proliferative status of the tumor cells. Overall, ciliated proliferating tumor cells are much more common in human tissue than previously appreciated. Future research will be required to clarify the factors that influence cilia expression *in vivo* and what role these organelles play in tumors beyond regulating SHH and Wnt signaling.

REFERENCES

1. Nevers Y, Prasad MK, Poidevin L, et al. Insights into Ciliary Genes and Evolution from Multi-Level Phylogenetic Profiling. *Mol Biol Evol*. 2017;34(8):2016-2034. doi:10.1093/molbev/msx146
2. Pazour GJ, Agrin N, Leszyk J, Witman GB. Proteomic analysis of a eukaryotic cilium. *J Cell Biol*. 2005;170(1):103-113. doi:10.1083/jcb.200504008
3. SOROKIN SP. Reconstructions of Centriole Formation and Ciliogenesis in Mammalian Lungs. *J Cell Sci*. 1968;3(2).
4. Huangfu D, Liu A, Rakeman AS, Murcia NS, Niswander L, Anderson K V. Hedgehog signalling in the mouse requires intraflagellar transport proteins. *Nature*. 2003;426(6962):83-87. doi:10.1038/nature02061
5. Rohatgi R, Milenkovic L, Scott MP. Patched1 Regulates Hedgehog Signaling at the Primary Cilium. *Science (80-)*. 2007;317(5836):372-376. doi:10.1126/science.1139740
6. Santos N, Reiter JF. A central region of Gli2 regulates its localization to the primary cilium and transcriptional activity. *J Cell Sci*. 2014;127(7):1500-1510. doi:10.1242/jcs.139253
7. Haycraft CJ, Banizs B, Aydin-Son Y, Zhang Q, Michaud EJ, Yoder BK. Gli2 and Gli3 Localize to Cilia and Require the Intraflagellar Transport Protein Polaris for Processing and Function. *PLoS Genet*. 2005;1(4):e53. doi:10.1371/journal.pgen.0010053
8. Tukachinsky H, Lopez L V, Salic A. A mechanism for vertebrate Hedgehog

signaling: recruitment to cilia and dissociation of SuFu-Gli protein complexes. *J Cell Biol*. 2010;191(2):415-428. doi:10.1083/jcb.201004108

9. Goetz SC, Anderson K V. The primary cilium: a signalling centre during vertebrate development. *Nat Rev Genet*. 2010;11(5):331-344. doi:10.1038/nrg2774
10. Corbit KC, Shyer AE, Dowdle WE, et al. Kif3a constrains β-catenin-dependent Wnt signalling through dual ciliary and non-ciliary mechanisms. *Nat Cell Biol*. 2008;10(1):70-76. doi:10.1038/ncb1670
11. Lancaster MA, Schroth J, Gleeson JG. Subcellular spatial regulation of canonical Wnt signalling at the primary cilium. *Nat Cell Biol*. 2011;13(6):700-707. doi:10.1038/ncb2259
12. Simons M, Gloy J, Ganner A, et al. Inversin, the gene product mutated in nephronophthisis type II, functions as a molecular switch between Wnt signaling pathways. *Nat Genet*. 2005;37(5):537-543. doi:10.1038/ng1552
13. Nauli SM, Alenghat FJ, Luo Y, et al. Polycystins 1 and 2 mediate mechanosensation in the primary cilium of kidney cells. *Nat Genet*. 2003;33(2):129-137. doi:10.1038/ng1076
14. Ocbina PJR, Tuson M, Anderson K V. Primary Cilia Are Not Required for Normal Canonical Wnt Signaling in the Mouse Embryo. Heisenberg C-P, ed. *PLoS One*. 2009;4(8):e6839. doi:10.1371/journal.pone.0006839
15. Huang P, Schier AF. Dampened Hedgehog signaling but normal Wnt signaling in zebrafish without cilia. *Development*. 2009;136(18):3089-3098. doi:10.1242/dev.041343

16. Kim M, Suh Y-A, Oh J-H, Lee BR, Kim J, Jang SJ. KIF3A binds to β-arrestin for suppressing Wnt/β-catenin signalling independently of primary cilia in lung cancer. *Sci Rep*. 2016;6(1):32770. doi:10.1038/srep32770

17. Dingemans KP. The relation between cilia and mitoses in the mouse adenohypophysis. *J Cell Biol*. 1969;43(2):361-367. http://www.ncbi.nlm.nih.gov/pubmed/5344153. Accessed December 19, 2018.

18. Tucker RW, Pardee AB, Fujiwara K. Centriole ciliation is related to quiescence and DNA synthesis in 3T3 cells. *Cell*. 1979;17(3):527-535. http://www.ncbi.nlm.nih.gov/pubmed/476831. Accessed December 19, 2018.

19. Kim S, Tsiokas L. Cilia and cell cycle re-entry: more than a coincidence. *Cell Cycle*. 2011;10(16):2683-2690. doi:10.4161/cc.10.16.17009

20. Spektor A, Tsang WY, Khoo D, Dynlacht BD. Cep97 and CP110 Suppress a Cilia Assembly Program. *Cell*. 2007;130(4):678-690. doi:10.1016/j.cell.2007.06.027

21. Pugacheva EN, Jablonski SA, Hartman TR, Henske EP, Golemis EA. HEF1-dependent Aurora A activation induces disassembly of the primary cilium. *Cell*. 2007;129(7):1351-1363. doi:10.1016/j.cell.2007.04.035

22. Kim S, Zaghloul NA, Bubenshchikova E, et al. Nde1-mediated inhibition of ciliogenesis affects cell cycle re-entry. *Nat Cell Biol*. 2011;13(4):351-360. doi:10.1038/ncb2183

23. Li A, Saito M, Chuang J-Z, et al. Ciliary transition zone activation of

phosphorylated Tctex-1 controls ciliary resorption, S-phase entry and fate of neural progenitors. *Nat Cell Biol*. 2011;13(4):402-411. doi:10.1038/ncb2218

24. Inoko A, Matsuyama M, Goto H, et al. Trichoplein and Aurora A block aberrant primary cilia assembly in proliferating cells. *J Cell Biol*. 2012;197(3):391-405. doi:10.1083/jcb.201106101

25. Pan J, Snell W. The Primary Cilium: Keeper of the Key to Cell Division. *Cell*. 2007;129(7):1255-1257. doi:10.1016/J.CELL.2007.06.018

26. Phua SC, Chiba S, Suzuki M, et al. Dynamic Remodeling of Membrane Composition Drives Cell Cycle through Primary Cilia Excision. *Cell*. 2017;168(1-2):264-279.e15. doi:10.1016/j.cell.2016.12.032

27. Sakaue-Sawano A, Kurokawa H, Morimura T, et al. Visualizing Spatiotemporal Dynamics of Multicellular Cell-Cycle Progression. *Cell*. 2008;132(3):487-498. doi:10.1016/j.cell.2007.12.033

28. Ford MJ, Yeyati PL, Mali GR, et al. A Cell/Cilia Cycle Biosensor for Single-Cell Kinetics Reveals Persistence of Cilia after G1/S Transition Is a General Property in Cells and Mice. *Dev Cell*. 2018;47(4):509-523.e5. doi:10.1016/j.devcel.2018.10.027

29. Hildebrandt F, Benzing T, Katsanis N. Ciliopathies. *N Engl J Med*. 2011;364(16):1533-1543. doi:10.1056/NEJMra1010172

30. Ma M, Gallagher A-R, Somlo S. Ciliary Mechanisms of Cyst Formation in Polycystic Kidney Disease. *Cold Spring Harb Perspect Biol*. 2017;9(11):a028209. doi:10.1101/cshperspect.a028209

31. Wheatley DN. Primary Cilia in Normal and Pathological Tissues. *Pathobiology*. 1995;63(4):222-238. doi:10.1159/000163955

32. Menzl I, Lebeau L, Pandey R, et al. Loss of primary cilia occurs early in breast cancer development. *Cilia*. 2014;3(1):7. doi:10.1186/2046-2530-3-7

33. Nobutani K, Shimono Y, Yoshida M, et al. Absence of primary cilia in cell cycle-arrested human breast cancer cells. *Genes Cells*. 2014;19(2):141-152. doi:10.1111/gtc.12122

34. Yuan K, Frolova N, Xie Y, et al. Primary cilia are decreased in breast cancer: analysis of a collection of human breast cancer cell lines and tissues. *J Histochem Cytochem*. 2010;58(10):857-870. doi:10.1369/jhc.2010.955856

35. Seeley ES, Carrière C, Goetze T, Longnecker DS, Korc M. Pancreatic cancer and precursor pancreatic intraepithelial neoplasia lesions are devoid of primary cilia. *Cancer Res*. 2009;69(2):422-430. doi:10.1158/0008-5472.CAN-08-1290

36. Hassounah NB, Nagle R, Saboda K, Roe DJ, Dalkin BL, McDermott KM. Primary cilia are lost in preinvasive and invasive prostate cancer. Glinskii VV, ed. *PLoS One*. 2013;8(7):e68521. doi:10.1371/journal.pone.0068521

37. Snedecor ER, Sung CC, Moncayo A, et al. Loss of Primary Cilia in Melanoma Cells is Likely Independent of Proliferation and Cell Cycle Progression. *J Invest Dermatol*. 2015;135(5):1456-1458. doi:10.1038/jid.2015.22

38. Egeberg DL, Lethan M, Manguso R, et al. Primary cilia and aberrant cell

signaling in epithelial ovarian cancer. *Cilia*. 2012;1(1):15. doi:10.1186/2046-2530-1-15

39. Gailani MR, Ståhle-Bäckdahl M, Leffell DJ, et al. The role of the human homologue of Drosophila patched in sporadic basal cell carcinomas. *Nat Genet*. 1996;14(1):78-81. doi:10.1038/ng0996-78
40. Taylor MD, Northcott PA, Korshunov A, et al. Molecular subgroups of medulloblastoma: the current consensus. *Acta Neuropathol*. 2012;123(4):465-472. doi:10.1007/s00401-011-0922-z
41. Han Y-G, Kim HJ, Dlugosz AA, Ellison DW, Gilbertson RJ, Alvarez-Buylla A. Dual and opposing roles of primary cilia in medulloblastoma development. *Nat Med*. 2009;15(9):1062-1065. doi:10.1038/nm.2020
42. Bay SN, Long AB, Caspary T. Disruption of the ciliary GTPase Arl13b suppresses Sonic hedgehog overactivation and inhibits medulloblastoma formation. *Proc Natl Acad Sci U S A*. 2018;115(7):1570-1575. doi:10.1073/pnas.1706977115
43. Wong SY, Seol AD, So P-L, et al. Primary cilia can both mediate and suppress Hedgehog pathway-dependent tumorigenesis. *Nat Med*. 2009;15(9):1055-1061. doi:10.1038/nm.2011
44. Amakye D, Jagani Z, Dorsch M. Unraveling the therapeutic potential of the Hedgehog pathway in cancer. *Nat Med*. 2013;19(11):1410-1422. doi:10.1038/nm.3389
45. Ran FA, Hsu PD, Wright J, Agarwala V, Scott DA, Zhang F. Genome engineering using the CRISPR-Cas9 system. *Nat Protoc*. 2013;8(11):2281-

2308. doi:10.1038/nprot.2013.143

46. Lin J-R, Fallahi-Sichani M, Sorger PK. Highly multiplexed imaging of single cells using a high-throughput cyclic immunofluorescence method. *Nat Commun*. 2015;6(1):8390. doi:10.1038/ncomms9390

47. Lin J-R, Izar B, Wang S, et al. Highly multiplexed immunofluorescence imaging of human tissues and tumors using t-CyCIF and conventional optical microscopes. *Elife*. 2018;7. doi:10.7554/eLife.31657

48. Schimmack S, Kneller S, Dadabaeva N, et al. Epithelial to Stromal Re-Distribution of Primary Cilia during Pancreatic Carcinogenesis. Rooman I, ed. *PLoS One*. 2016;11(10):e0164231. doi:10.1371/journal.pone.0164231

49. Kobayashi T, Nakazono K, Tokuda M, Mashima Y, Dynlacht BD, Itoh H. HDAC2 promotes loss of primary cilia in pancreatic ductal adenocarcinoma. *EMBO Rep*. 2017;18(2):334-343. doi:10.15252/embr.201541922

50. Domcke S, Sinha R, Levine DA, Sander C, Schultz N. Evaluating cell lines as tumour models by comparison of genomic profiles. *Nat Commun*. 2013;4(1):2126. doi:10.1038/ncomms3126

51. Cowley GS, Weir BA, Vazquez F, et al. Parallel genome-scale loss of function screens in 216 cancer cell lines for the identification of context-specific genetic dependencies. *Sci Data*. 2014;1:140035. doi:10.1038/sdata.2014.35

52. Meyers RM, Bryan JG, McFarland JM, et al. Computational correction of copy number effect improves specificity of CRISPR-Cas9 essentiality

screens in cancer cells. *Nat Genet*. 2017;49(12):1779-1784. doi:10.1038/ng.3984

53. Hoang-Minh LB, Dutra-Clarke M, Breunig JJ, Sarkisian MR. Glioma cell proliferation is enhanced in the presence of tumor-derived cilia vesicles. *Cilia*. 2018;7(1):6. doi:10.1186/s13630-018-0060-5

54. Jenks AD, Vyse S, Wong JP, et al. Primary Cilia Mediate Diverse Kinase Inhibitor Resistance Mechanisms in Cancer. *Cell Rep*. 2018;23(10):3042-3055. doi:10.1016/j.celrep.2018.05.016

55. Coy S, Du Z, Sheu S-H, et al. Distinct patterns of primary and motile cilia in Rathke's cleft cysts and craniopharyngioma subtypes. *Mod Pathol*. 2016;29(12):1446-1459. doi:10.1038/modpathol.2016.153

56. Zingg D, Debbache J, Peña-Hernández R, et al. EZH2-Mediated Primary Cilium Deconstruction Drives Metastatic Melanoma Formation. *Cancer Cell*. 2018;34(1):69-84.e14. doi:10.1016/j.ccell.2018.06.001

57. Ma R, Li W-P, Rundle D, Kong J, Akbarali HI, Tsiokas L. PKD2 functions as an epidermal growth factor-activated plasma membrane channel. *Mol Cell Biol*. 2005;25(18):8285-8298. doi:10.1128/MCB.25.18.8285-8298.2005

58. Schneider L, Clement CA, Teilmann SC, et al. PDGFRalphaalpha signaling is regulated through the primary cilium in fibroblasts. *Curr Biol*. 2005;15(20):1861-1866. doi:10.1016/j.cub.2005.09.012

59. Moser JJ, Fritzler MJ, Rattner JB. Ultrastructural characterization of primary cilia in pathologically characterized human glioblastoma multiforme (GBM) tumors. *BMC Clin Pathol*. 2014;14(1):40. doi:10.1186/1472-6890-

14-40

FIGURES

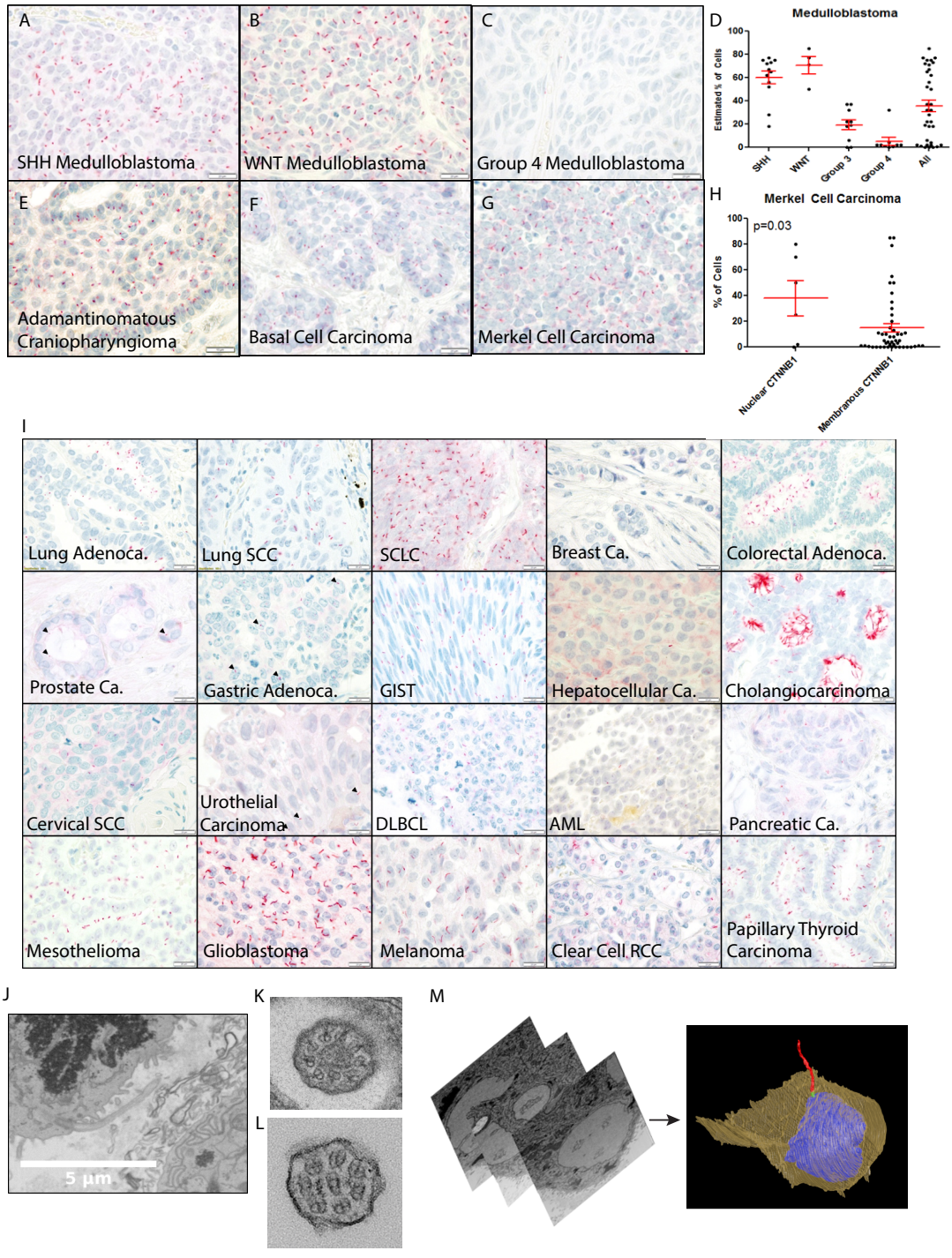

Figure 1. Cilia are expressed across the spectrum of human cancers. Representative images of ARL13b IHC of A) SHH-driven medulloblastoma, B) Wnt medulloblastoma, and C) Group 4 medulloblastoma and D) quantification of frequency of ciliated cells in medulloblastoma cases (n=35). Representative ARL13b IHC images of E) adamantinomatous craniopharyngioma, F) basal cell

carcinoma, and G) Merkel cell carcinoma with H) quantification of frequency of ciliated cells in Merkel cell carcinoma cases grouped by IHC beta-catenin staining pattern. I) Representative ARL13b IHC images of lung adenocarcinoma, lung squamous cell carcinoma (SCC), small cell lung carcinoma (SCLC), breast carcinoma, colorectal adenocarcinoma, prostate carcinoma, gastric adenocarcinoma, gastrointestinal stromal tumor (GIST), hepatocellular carcinoma, cholangiocarcinoma, cervical squamous cell carcinoma (SCC), urothelial carcinoma, diffuse large B-cell lymphoma (DLBCL), acute myeloid leukemia (AML), pancreatic cancer, mesothelioma, glioblastoma, melanoma, clear cell renal cell carcinoma, and papillary thyroid cancer. J) FIB-SEM showing TEM of a longitudinal view of cilium on an OVSAHO ovarian cancer PDX tumor cell. K) Canonical 9+0 axoneme cross-sectional view, with central electron density likely representing the terminal plate of the transition zone. L) Non-canonical 7+3 axoneme on Kuramochi ovarian cancer cells. M) 3D reconstruction of OVASAHO PDX tumor cell using serial TEM micrographs, blue=nucleus, yellow=cytoplasm, green=basal body, red=cilium.

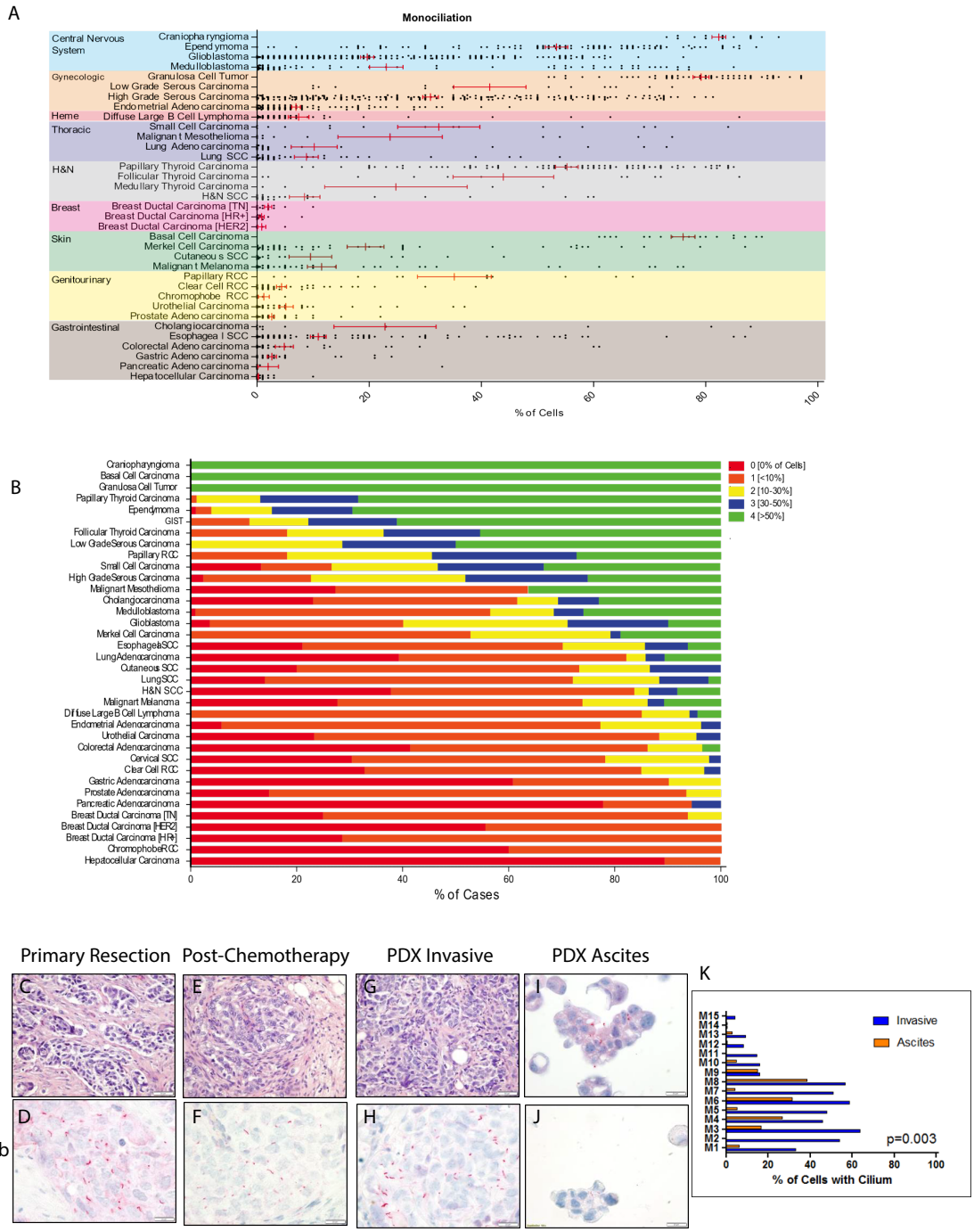

Figure 2. Frequency of ciliation is heterogeneous within tumor types and is maintained after chemotherapy and in PDX models. A) Quantification of percentage of cells with cilia showing individual tumor cases, grouped by organ system. B) Percentage of cases low to high degrees of ciliation. C-D) H&E and ARL13b IHC of a primary omental tumor resection of high grade serous ovarian carcinoma before treatment, as well as E-F) after treatment with carboplatin and paclitaxel. G-H) H&E and ARL13b IHC of an ovarian cancer PDX tumor grown as

an invasive model in the mouse omentum. I-J) Representative ARL13b IHC images of ovarian cancer PDX tumor grown as ascites in the mouse. K) Quantification of percent ciliation in PDX tumors.

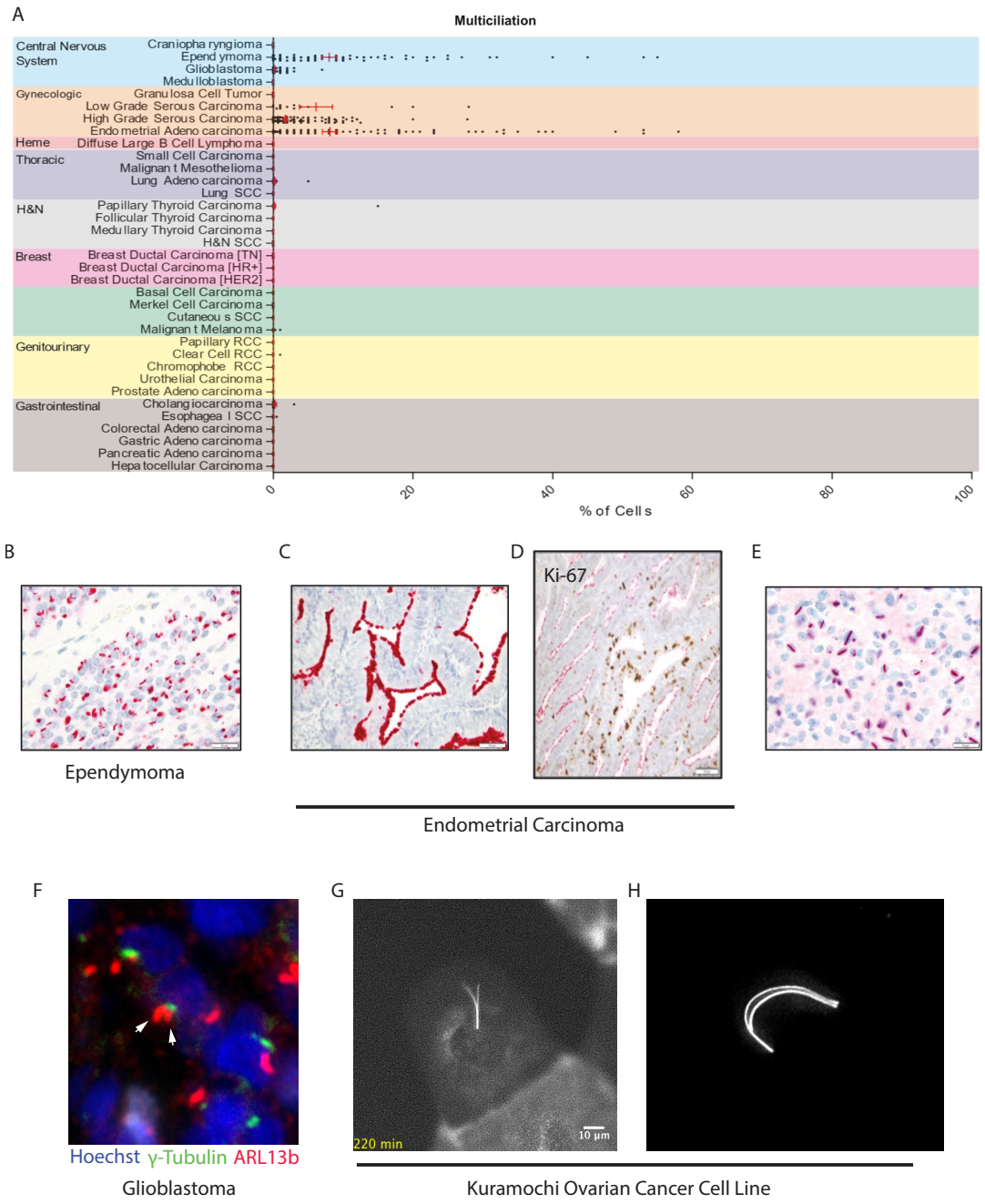

Figure 3. Multiciliated tumor cells are found in multiple tumor types. A) Quantification of multiciliated cells in human tumors, by organ system. Representative ARL13b IHC images of B) ependymoma and C) endometrial adenocarcinoma. D) IHC double stain of endometrial adenocarcinoma with ARL13b (red) and Ki-67 (brown). E) ARL13b IHC of oligodendroglioma showing linear structures spanning the nuclei. F) Tissue immunofluorescence of glioblastoma showing biciliate tumor cells. ARL13b-eGFP expressing Kuramochi ovarian cancer cells with 2 cilia, shown by G) conventional wide-field

epifluorescence microscopy and H) high-resolution maximal intensity projection images.

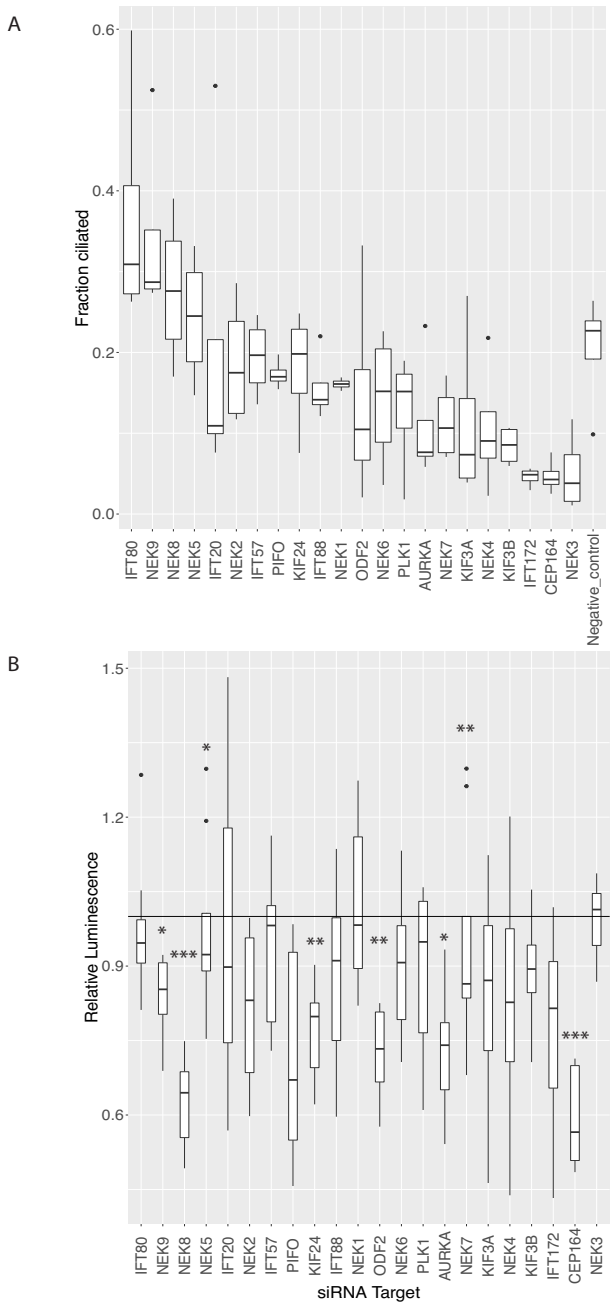

Figure 4. siRNA directed against genes related to cilia result in variable degrees of cilia reduction and changes in proliferation. A) Quantification of fraction of ciliated Kuramochi ovarian cancer cells 48 hours after siRNA transfection. B) Relative luminescence by CellTiter Glo assay as compared to the negative control siRNA (horizontal line) 72 hours after siRNA transfection, n=4 replicates. * $p \leq 0.05$, ** $p \leq 0.01$, *** $p \leq 0.001$.

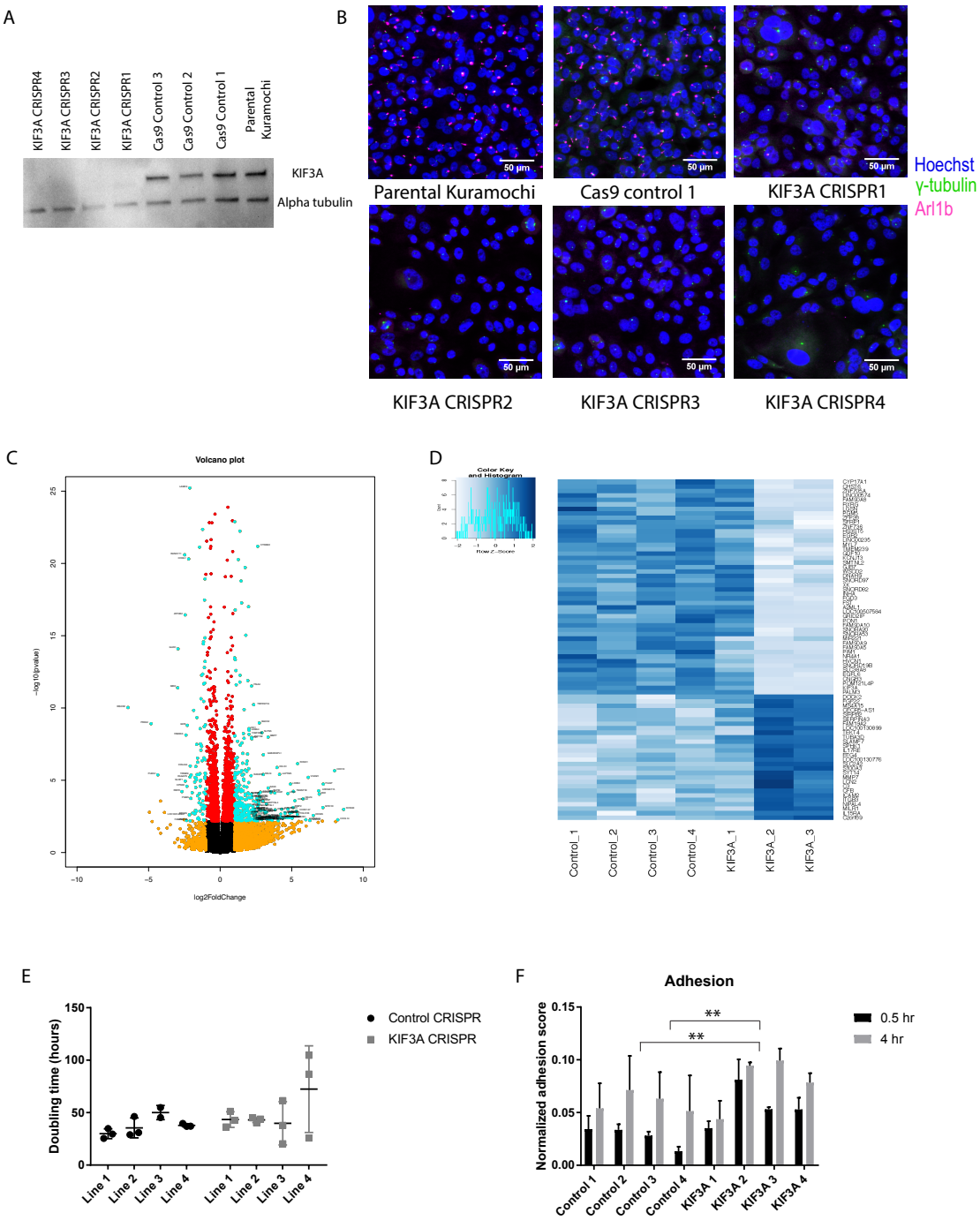

Figure 5. KIF3A CRISPR-mediated cilia knockout in ovarian cancer cells results in changes in cell adhesion gene RNA levels but does not alter cell proliferation. A) Western blot of monoclonally-derived KIF3A CRISPR Kuramochi ovarian cancer cell lines. B) Representative immunofluorescence images of fixed Kuramochi cells after 72 hours of serum starvation. C) Volcano plot of RNA sequencing results, showing differentially expressed genes between

KIF3A knockout (mean of KIF3A CRISPR 2 and KIF3A CRISPR 3) and control cell lines. Gene transcripts with > 2 fold change shown in orange, transcripts with statistically significant changes ($q < 0.05$) in red, and both of the above in cyan. D) Heatmap showing transcripts that were either upregulated or downregulated at statistical significance ($q < 0.05$) in the complete KIF3A knockout lines (KIF3A CRISPR 2 and KIF3A CRISPR 3) versus the control cell lines. E) Doubling times of the KIF3A CRISPR and control cell lines, measured over 72 hours under normal growth conditions. F) Relative cell adhesion at 30 minutes and 4 hours after seeding into tissue-coated plates. ** $p \leq 0.01$.

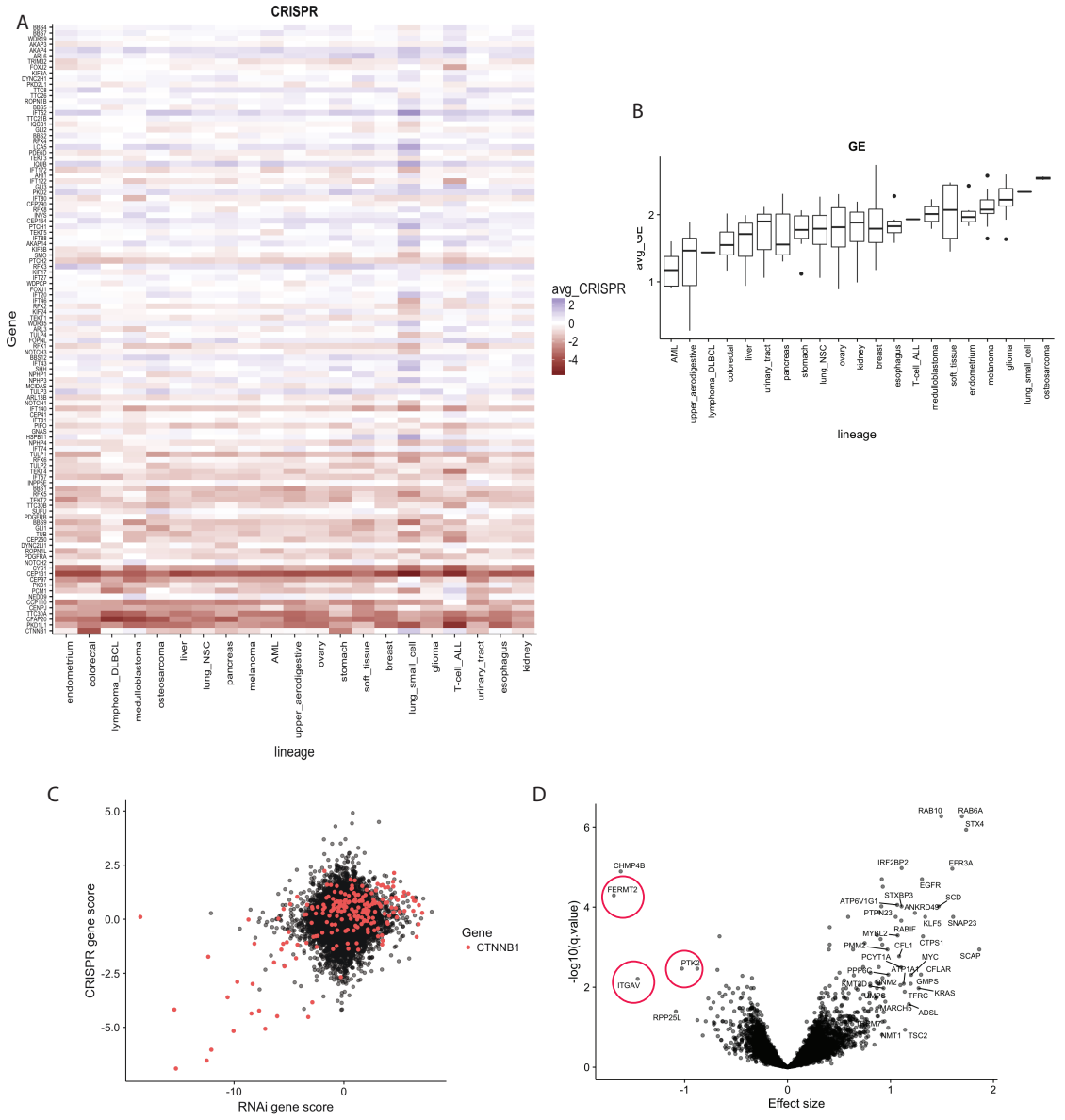

Figure 6. Project Achilles cell line data shows dependency on beta-catenin in select tumors and identifies dependency on cell adhesion genes in cell lines expressing high levels of cilia genes. Genes were knocked down using either shRNA (n=501 cell lines) or CRISPR (Ach 3.3.8 and avana_public_18Q1) and assigned a Z-MAD normalized gene score reflecting relative cell abundance using next generation sequencing. Negative gene scores indicate greater killing/less growth of cells upon knockout of the corresponding gene. A) Heatmap of cilia averaged CRISPR gene scores across different human cancer cell lines by lineage type. B) Averaged relative gene expression (GE) of the cilia gene set across different cancer cell line lineage types. C) Gene scores from shRNA-mediated knockdown versus CRISPR-mediated knockdown, each point representing a particular cilia-related gene and individual cell line. D) Volcano plot of effect size (correlation between increased cilia gene expression and gene

score) versus statistical significance for the CRISPR dataset. Negative effect size values reflect decreased gene scores with higher cilia gene expression, indicating greater dependency. PTK2, ITGAV, and FERMT2 are cellular adhesion-related genes and are circled.

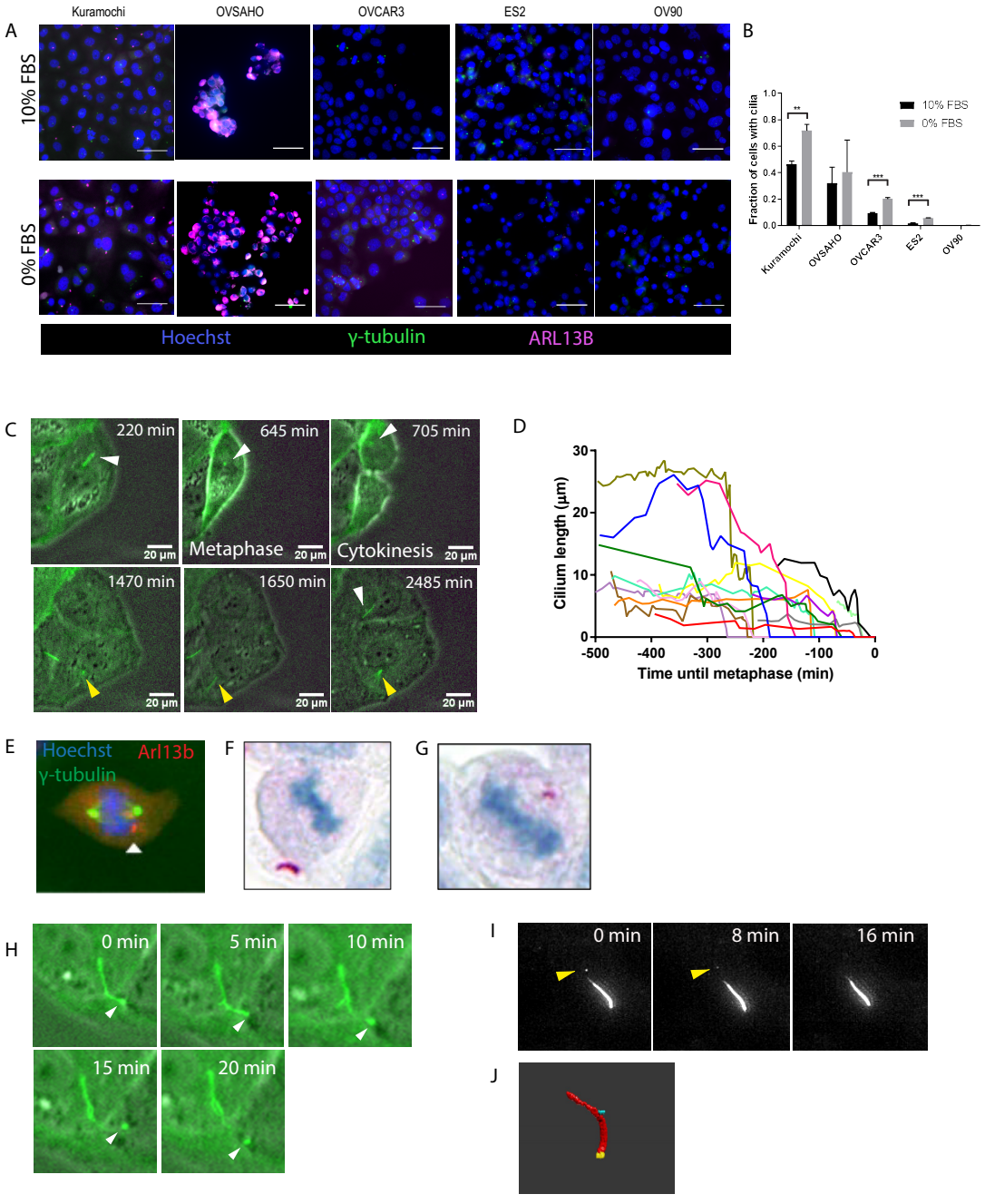

Figure 7. In ovarian cancer cell lines, cilia are dynamically expressed in proliferating cells. A) Representative immunofluorescence images of ovarian cancer cell lines before and after serum starvation for 72 hours. γ-tubulin marks basal bodies, scale bar = 50 um. B) Quantification of cilia in ovarian cancer cell lines. Error bars represent SEM, * $p \leq 0.05$, ** $p \leq 0.01$, *** $p \leq 0.001$. C) Representative still images from live cell imaging of ARL13b-eGFP expressing Kuramochi ovarian cancer cells illustrating cell division with cilia disassembly and reassembly. Images show GFP fluorescence (green) merged with brightfield

images (grayscale). White arrowheads = cilium of the parent cell and upper daughter cell. Yellow arrowheads = cilium of the lower daughter cell. D) Cilia length measured by live cell imaging in individual ARL13b-eGFP Kuramochi cells in relation to mitosis (metaphase t=0, n=15). E) Immunofluorescence of a fixed Kuramochi cell and F-G) ARL13b IHC of high grade serous ovarian carcinoma cells undergoing mitosis with a cilium present. H) Representative still images of ARL13b-eGFP expressing OVSAHO ovarian cancer cells. White arrowheads illustrate ciliary tip excision in a biciliate cell. I) High-resolution maximal intensity projection images of Kuramochi ARL13b-eGFP cilia depicting tip excision (yellow arrowheads). J) FIB-SEM serial image-based 3D reconstruction of an OVSAHO PDX tumor cell cilium (red) and basal body (yellow) with an associated vesicle (cyan).

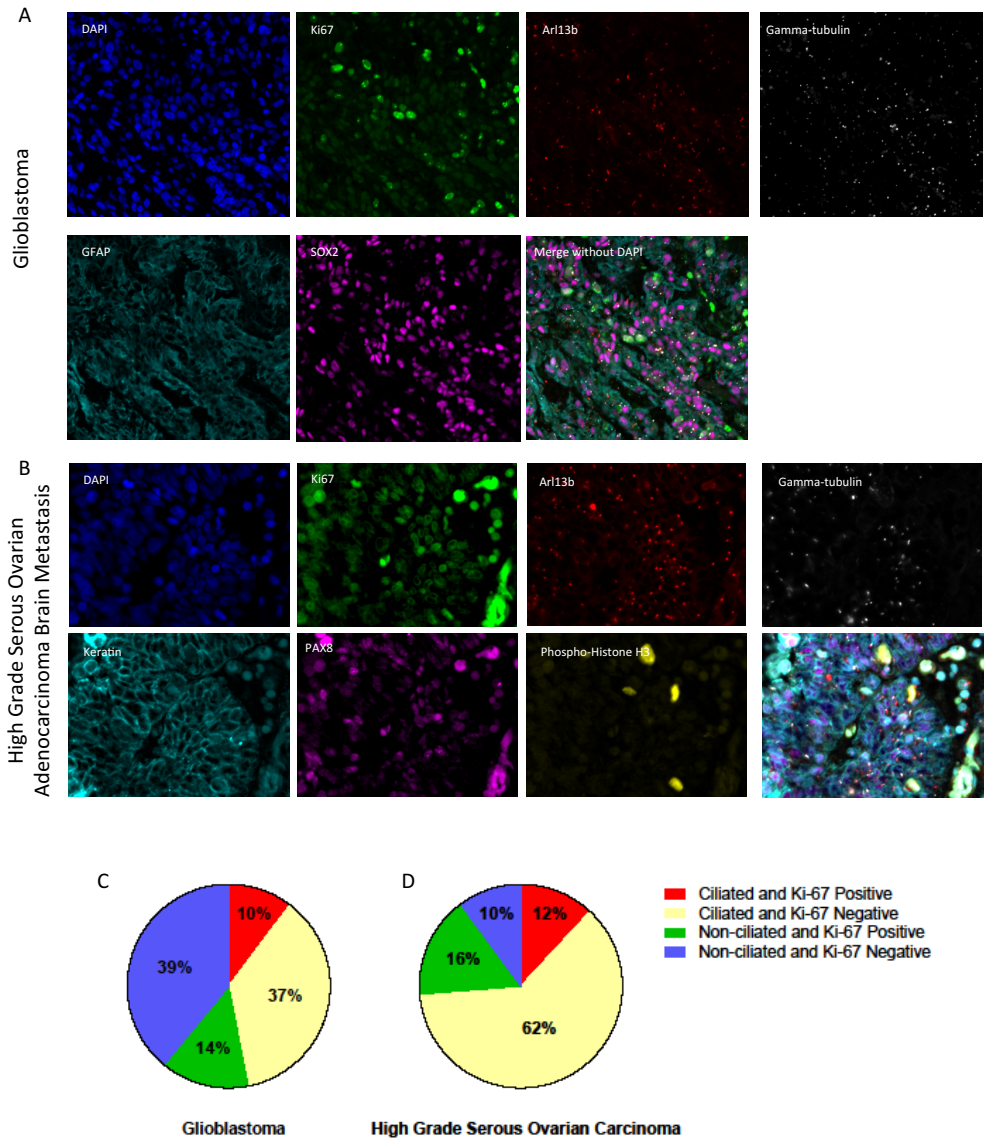

Figure 8. Single-cell immunofluorescence characterization of human glioblastoma and high grade serous ovarian carcinoma tissue shows solitary cilia are expressed by actively proliferating tumor cells. Representative t-CyCIF images of one 20X field view each of A) a glioblastoma case and B) a high grade serous ovarian adenocarcinoma brain metastasis, with C-D) quantification of tumor cells with or without cilia and Ki-67 expression status.

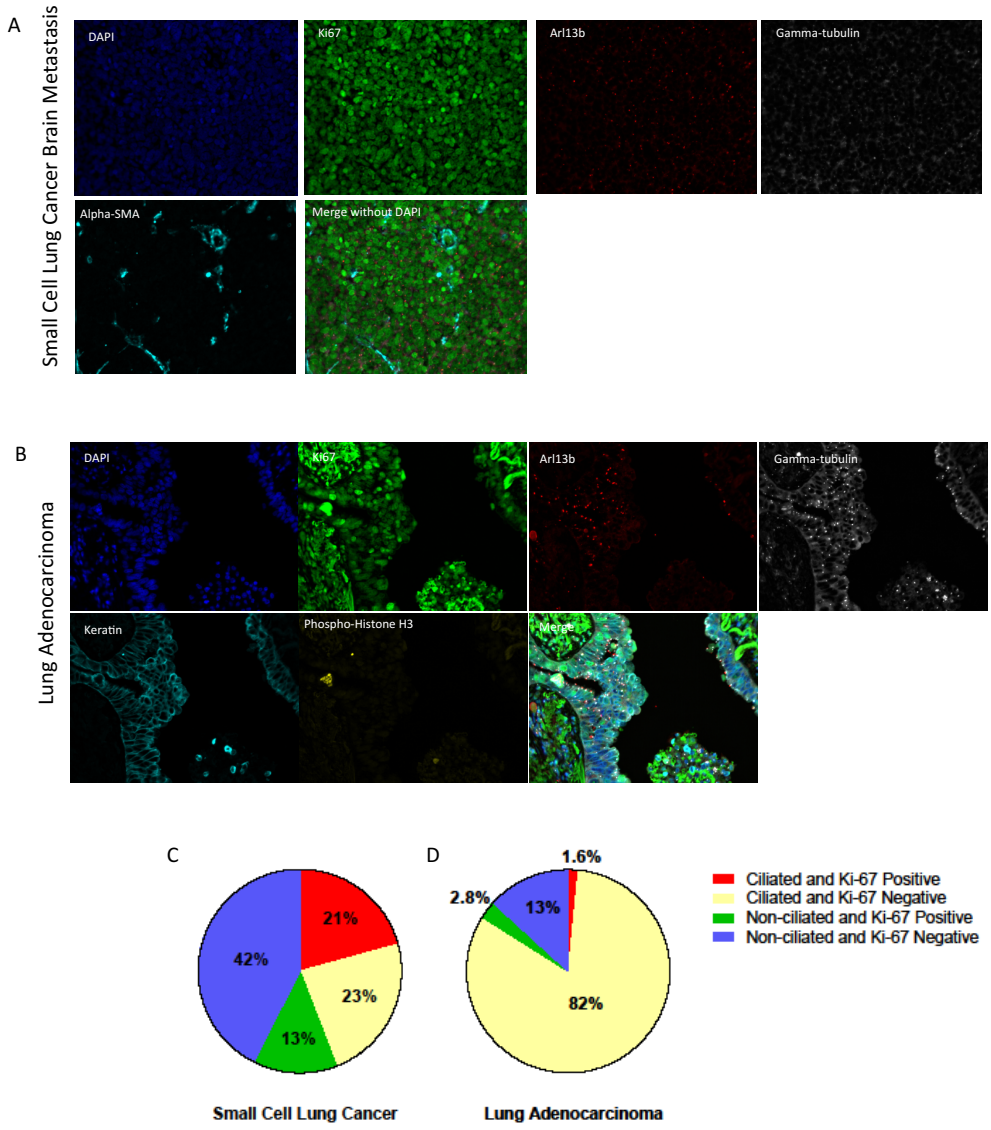

Figure 9. Single-cell immunofluorescence characterization of lung adenocarcinoma and SCLC tissue shows solitary cilia are expressed by actively proliferating tumor cells. Representative t-CyCIF images of one 20X field view each of A) a SCLC brain metastasis and B) a lung adenocarcinoma primary tumor, with C-D) quantification of tumor cells with or without cilia and Ki-67 expression status.

SUPPLEMENTARY VIDEOS AND TABLES

Supplementary Video 1. Live cell imaging of ARL13b-eGFP Kuramochi cells undergoing mitosis with cilia disassembly and reassembly

Supplementary Video 2. De-convoluted maximal intensity projection live cell imaging of ciliary tip excision in an ARl13b-eGFP Kuramochi cell

Supplementary Table 1. KIF3A CRISPR guide RNA sequences (5' to 3')

sgRNA name	Guide sequence	Forward oligonucleotide	Reverse oligonucleotide
KIF3A guide 1	AGCTACTGGACAGCGCCT AAAGG	CACCGAGCTACTGG ACAGCGCCTAA	AAACTTAGGCGCTG TCCAGTAGCTC
KIF3A guide 2	GTCAGTTTAGAGTTACGAT AAGG	CACCGGTCAGTTTA GAGTTACGATA	AAACTATCGTAACT CTAAACTGACC
KIF3A guide 3	AGAACATTCGGCAACTTAG CCGG	CACCGAGAACATTC GGCAACTTAGC	AAACGCTAAGTTGC CGAATGTTCTC

Supplementary Table 2. Antibodies used for t-CyCIF on human tumors

Protein Target	Vendor	Catalog #	Dilution
ARL13b	Antibodies Inc.	75-287	1:100
Ɣ-tubulin	Abcam	ab191114	1:100
PCNA	Cell Signaling Technologies	8580	1:100
Ki-67	Cell Signaling Technologies	12160S	1:100
Phospho-histone H3	Cell Signaling Technologies	3475	1:100
Pan-cytokeratin	eBioscience	41-9003-80	1:500
SOX2	Cell Signaling Technologies	5179	1:100
GFAP	eBioscience	41-9892-80	1:100
CD45	Biolegend	304056	1:100
α-smooth muscle actin (α-SMA)	eBioscience	50-9760-80	1:100

Supplementary Table 3. siRNA target genes and sequences

Gene	Sense siRNA	Antisense siRNA
KIF3A	CCUCCAAAGACAUUUACUUtt	AAGUAAAUGUCUUUGGAGGtt
KIF3A	GGUGUUCGAGCUAUUCCUGtt	CAGGAAUAGCUCGAACACCtt
KIF3A	GGCUACAAUGGGACUAUUUtt	AAAUAGUCCCAUUGUAGCCtt
IFT88	GGAAUUGGAGAAUGAUGCAtt	UGCAUCAUUCUCCAAUUCCtc
IFT88	GAAGUGGUAACUACCAAAAtt	UUUUGGUAGUUACCACUUCtt
IFT88	CCUAUAGCUACUGGAUAUGtt	CAUAUCCAGUAGCUAUAGGtc
IFT172	CCGAGUGGUCUUGCUGUAUtt	AUACAGCAAGACCACUCGGtc
IFT172	GGUUCGUUUAGCAAACACCtt	GGUGUUUGCUAAACGAACCtt
IFT172	GGUCACAUGCUACAAACUUtt	AAGUUUGUAGCAUGUGACCtt
KIF3B	CCUUUGAUGCCGUCUAUGAtt	UCAUAGACGGCAUCAAAGGtg
KIF3B	GCAGUUUGAACUGUACGAUtt	AUCGUACAGUUCAAACUGCtt
KIF3B	CCAAAAAACUCAAAAAGCUtt	AGCUUUUUGAGUUUUUUGGtc
IFT20	GGUUACCCAGCAGACCAUAtt	UAUGGUCUGCUGGGUAACCtc
IFT20	GGAAGAGUGCAAAGACUUUtt	AAAGUCUUUGCACUCUUCCtt
IFT20	GCAGACCAUAGAGCUGAAGtt	CUUCAGCUCUAUGGUCUGCtg
IFT57	GGAGUGACGGAAAGAACCAtt	UGGUUCUUUCCGUCACUCCtc
IFT57	GCUUCGGUCAUUUGGAAGAtt	UCUUCCAAAUGACCGAAGCtc
IFT57	GGUGCAUAUGCAUGUCUCAtt	UGAGACAUGCAUAUGCACCtt
IFT80	GGCAGAAAGCUUUGUCCUCtt	GAGGACAAAGCUUUCUGCCtg
IFT80	GGUAUGGGAUAGUUACGGCtt	GCCGUAACUAUCCCAUACCtt
IFT80	CGAUACAUGCAAUAUCCUUtt	AAGGAUAUUGCAUGUAUCGtt
CEP164	GGAACCAGAACUGAUGUGGtt	CCACAUCAGUUCUGGUUCCtt
CEP164	GGACAUCACAGGUGACAUUtt	AAUGUCACCUGUGAUGUCCtg
CEP164	CAGAGUUCACCAGAAGUCUtt	AGACUUCUGGUGAACUCUGtg
PLK1	GGUUUUCGAUUGCUCCCAGtt	CUGGGAGCAAUCGAAAACCtt
PLK1	GGAGGUGUUCGCGGGCAAGtt	CUUGCCCGCGAACACCUCCtt
PLK1	GGUGGAUGUGUGGUCCAUUtt	AAUGGACCACACAUCCACCtc
KIF24	GGCAUUAAGUGUUGCACUUtt	AAGUGCAACACUUAAUGCCtt
KIF24	GCAGCUUGUGUCUCGAGUUtt	AACUCGAGACACAAGCUGCtt
KIF24	GGUUUAAAAGACUCAGUCUtt	AGACUGAGUCUUUUAAACCtg
ODF2	GGUCACUGUAAAAUGAACCtt	GGUUCAUUUUACAGUGACCtg
ODF2	GGUCAAGAUGCAAAAAGGUtt	ACCUUUUUGCAUCUUGACCtc
ODF2	GGAUUCUGAAAGACUAAUGtt	CAUUAGUCUUUCAGAAUCCtc
AURKA	GGUCCAAAACGUGUUCUCGtt	CGAGAACACGUUUUGGACCtc
AURKA	GGAACUGGCAUCAAAACAGtt	CUGUUUUGAUGCCAGUUCCtc
AURKA	GGCAACCAGUGUACCUCAUtt	AUGAGGUACACUGGUUGCCtg
NEK1	GCUGGCUCGAACUUGCAUAtt	UAUGCAAGUUCGAGCCAGCtc
NEK1	GGUUUUAUAGCCAAACGCAtt	UGCGUUUGGCUAUAAAACCtt
NEK1	GCGAGAAAUACUUCGUAGAtt	UCUACGAAGUAUUUCUCGCtt
NEK2	GGAAGAGUGAUGGCAAGAUtt	AUCUUGCCAUCACUCUUCCtc
NEK2	GGGAACCAAGGAAAGGCAAtt	UUGCCUUUCCUUGGUUCCCtt
NEK2	GGAUGUUAAACUUAAAGGAtt	UCCUUUAAGUUUAACAUCCtc
NEK3	GGAGGCUGUUCUUUUAGCCtt	GGCUAAAAGAACAGCCUCCtt
NEK3	GGCAAAUAGUUGGAAAAAUtt	AUUUUUCCAACUAUUUGCCtg
NEK3	GCAGUAAUCAGAUGUUUGCtt	GCAAACAUCUGAUUACUGCtt
NEK4	GGAGUCAUGGGAAGGAGGAtt	UCCUCCUUCCCAUGACUCCtt
NEK4	GGACAAAUCUGUUGUUUGUtt	ACAAACAACAGAUUUGUCCtc
NEK4	GGAAGCCCAGCUCUUGUCUtt	AGACAAGAGCUGGGCUUCCtg

NEK5	GGAAAUACGCCAACAGUACtt	GUACUGUUGGCGUAUUUCCtc
NEK5	GGUGGUCCAGAAGUGUAAAtt	UUUACACUUCUGGACCACCtt
NEK5	CCGACCAUCCAUAAAUUCCtt	GGAAUUUAUGGAUGGUCGGtc
NEK6	GGCAUCCCAACACGCUGUCtt	GACAGCGUGUUGGGAUGCCtc
NEK6	GGAUUGCUGACAGACAGAAtt	UUCUGUCUGUCAGCAAUCCtg
NEK6	GCACUACUCCGAGAAGUUAtt	UAACUUCUCGGAGUAGUGCtc
NEK7	GGCUAAUUCCUGAAAGAACtt	GUUCUUUCAGGAAUUAGCCtc
NEK7	GUACCAGUAGCUUUAAAAAtt	UUUUUAAAGCUACUGGUACtc
NEK7	GUAGCUUUAAAAAAAGUGCtt	GCACUUUUUUUAAAGCUACtg
NEK8	GGCAUCAUCAUGACAUUCGtt	CGAAUGUCAUGAUGAUGCCtc
NEK8	GGAAGCUCAGCGAGUUGUAtt	UACAACUCGCUGAGCUUCCtg
NEK8	GGAGCCUCUGCUGAGUAUAtt	UAUACUCAGCAGAGGCUCCtg
NEK9	GGAAGUCGAUUUGACCCGGtt	CCGGGUCAAAUCGACUUCCtt
NEK9	GGAGUAAAGUACAAUUUCAtt	UGAAAUUGUACUUUACUCCtt
NEK9	GGAUGACUCACUGGUUGUGtt	CACAACCAGUGAGUCAUCCtc
PIFO	GGUUUAAGCCAAUACAGAAtt	UUCUGUAUUGGCUUAAACCtc
PIFO	GGACACUUACUAUCCCAGCtt	GCUGGGAUAGUAAGUGUCCtt
PIFO	GCUGUGAGGUUUAAGCCAAtt	UUGGCUUAAACCUCACAGCtg